

# Time optimal control of a two-level dissipative quantum system

D. Sugny,\* C. Kontz, and H. R. Jauslin

*Institut Carnot, UMR CNRS 5027, BP 47870, 21078 Dijon, France*

(Dated: October 23, 2018)

## Abstract

We propose an analysis of the time-optimal control of a dissipative two-level quantum system whose dynamics is governed by the Lindblad equation. This simple system allows one to use tools of geometric control theory and to construct its optimal synthesis i.e. to determine the set of all the optimal trajectories starting from a given initial point. We study different processes such as conversion of a pure state into a mixed-state and purification of a mixed-state. In particular cases, we show that dissipation is not undesirable and can help accelerating the control.

PACS numbers: 32.80.Qk,03.65.Yz,78.20.Bh

arXiv:0708.3794v1 [quant-ph] 28 Aug 2007

---

\*Electronic address: dominique.sugny@u-bourgogne.fr

## I. INTRODUCTION

Manipulating quantum system by using time-dependent electric field remains a goal of primary interests in different physical processes extending from the control of chemical reactions [1, 2, 3] to quantum computing [4]. In recent years, active research has been performed to take into account the interaction of the system with the environment which represents more realistic situations but also more challenging control scenarios than for closed quantum systems [5, 6, 7]. Different control strategies have been proposed. In this paper we will not consider control techniques using non-unitary control such as measurement (see for instance the quantum Zeno effect) [8, 9, 10, 11, 12, 13, 14], or other strategies such as bang-bang pulses, strong coupling with another system or control that can actively act on the dissipation (see [15] for a recent review and references therein). It has been shown that such methods are particularly efficient and can even halt decoherence. We restrict our study to unitary control. In this case and for the interaction with a markovian or a non-markovian bath, the fact that the control field cannot fully compensate the effect of dissipation largely enhances the difficulty of the control. This point has been rigourously shown in Refs. [16, 17] for a dynamics governed by the Lindblad equation [18, 19]. In this context, several studies using numerical optimization techniques have proved that efficient control can still be achieved [20, 21, 22, 23, 24, 25, 26]. Due to the complexity of realistic systems with multiple degrees of freedom, this purely numerical approach seems to be the only possible way to achieve control. More geometrical aspects of the control using mainly tools of geometric control theory [27, 28, 29] can be formulated only for simplest quantum systems having few levels (typically two or three) or consisting in the coupling of spin 1/2 particles. This has been done recently by a large number of mathematical papers dealing with closed [30, 31, 32, 33, 34, 35, 36, 37, 38, 39] or dissipative [40] quantum systems. One of the objectives of the control has been the minimization of the total time of the process either with constraints [30, 33] or no constraints on the laser intensity [34].

In this paper, we propose to do a step towards the geometrical analysis of the control of dissipative quantum systems by beginning with the simplest system possible, a two-level system governed by the Lindblad equation. We determine control fields which minimize the total time of the process by applying the Pontryagin maximum principle (PMP) [27, 28, 29, 41]. The maximum of the laser intensity is fixed to an arbitrary value. An increase

of this value leads to a reduction of the duration of the control. Note also that this cost functional seems particularly relevant in the context of a dissipative environment especially when the effect of dissipation is undesirable to reach the objective of the control. A second argument explaining our choice of cost functional is of mathematical nature. The resolution of the PMP is particularly simple in this case and can be done analytically. The geometrical description of the time-optimal control is also well developed especially on  $\mathbb{R}^2$  (see [28] for a recent overview) for affine systems with a drift term corresponding here to the dissipation. The main tools of this construction will be recalled throughout the paper. Finally, all this mathematical arsenal allows us to answer some physical questions such as the benefit that can be gained from dissipation.

The paper is organized as follows. We first introduce the model for the Lindblad equation of a two-level system. Writing the density matrix in the coherence vector form [42] and assuming some constraints on the control term, we restrict the problem to a control on a closed submanifold of  $\mathbb{R}^2$  with a true drift term i.e. an uncontrollable term which cannot be eliminated by a unitary transformation. This drift term is due to the dissipation. We consider different cases with different initial and target states that represent several situations of physical interest. We formulate in Sec. III the PMP with a time minimum cost functional. In Sec. IV, we analyze the structure of the reachable set from each initial state and we point out the particular role of the fixed point of the free-dynamics in this structure. Section V deals with the construction of the optimal syntheses by solving the PMP. We recall that the PMP allows us to derive extremal controls. Optimal trajectories are a subset of this set which can be determined in a second step by a direct comparison of different extremal trajectories or by geometrical arguments. Conclusions and prospective views are given in Sec. VI. Some technical calculations are reported in appendices A and B.

## II. THE MODEL SYSTEM

We consider a dissipative two-level quantum system whose dynamics is governed by the Lindblad equation. The system is described by a density operator  $\rho(t)$  which is a positive semi-definite hermitian operator acting on a two-dimensional Hilbert space  $\mathcal{H}$ . The evolution equation can be written as

$$i\frac{\partial\rho}{\partial t} = [H_0 + uH_1, \rho] + i\mathcal{L}_D(\rho) , \quad (1)$$

where  $H_0$  is the field-free Hamiltonian of the system,  $H_1$  represents the interaction with the control field and  $\mathcal{L}_D$  the dissipative part of the equation. In the Lindblad equation,  $\mathcal{L}_D$  can be written in the general form

$$\sum_{k=1}^3 [L_k \rho L_k^\dagger - \frac{1}{2}(\rho L_k^\dagger L_k + L_k^\dagger L_k \rho)] , \quad (2)$$

where the operators  $L_k$  are given by

$$L_1 = \sqrt{\gamma_{21}} \begin{pmatrix} 0 & 1 \\ 0 & 0 \end{pmatrix}; L_2 = \sqrt{\gamma_{12}} \begin{pmatrix} 0 & 0 \\ 1 & 0 \end{pmatrix}; L_3 = \sqrt{\tilde{\Gamma}} \begin{pmatrix} 1 & 0 \\ 0 & -1 \end{pmatrix} . \quad (3)$$

$\gamma_{12}$ ,  $\gamma_{21}$  and  $\tilde{\Gamma}$  are positive real constants describing the interaction with the environment.  $\gamma_{12}$  and  $\gamma_{21}$  correspond to population relaxations whereas  $\tilde{\Gamma}$  is the pure dephasing rate. We consider resonant fields, i.e. the frequency  $\omega$  of the laser is equal to the energy difference between the two levels. In the RWA approximation, the time evolution of  $\rho(t)$  satisfies the following Redfield form of the Lindblad equation

$$i \frac{\partial}{\partial t} \begin{pmatrix} \rho_{11} \\ \rho_{12} \\ \rho_{21} \\ \rho_{22} \end{pmatrix} = \begin{pmatrix} -i\gamma_{12} & -u^* e^{-i\omega t} & u e^{i\omega t} & i\gamma_{21} \\ -u e^{i\omega t} & -\omega - i\Gamma & 0 & u e^{i\omega t} \\ u^* e^{-i\omega t} & 0 & \omega - i\Gamma & -u^* e^{-i\omega t} \\ i\gamma_{12} & u^* e^{-i\omega t} & -u e^{i\omega t} & -i\gamma_{21} \end{pmatrix} \begin{pmatrix} \rho_{11} \\ \rho_{12} \\ \rho_{21} \\ \rho_{22} \end{pmatrix} , \quad (4)$$

where  $u$  is the complex Rabi frequency of the laser field (the real and imaginary parts are the amplitudes of two orthogonal linearly polarized fields).  $\Gamma$  is the total dephasing rate which can be written as

$$\Gamma = \frac{1}{2}(\gamma_{12} + \gamma_{21}) + \tilde{\Gamma} . \quad (5)$$

From Eqs. (5), we also notice that the requirement that Eq. (4) corresponds to a Lindblad equation implies the constraint  $\Gamma \geq \frac{1}{2}(\gamma_{12} + \gamma_{21})$  or equivalently  $\tilde{\Gamma} \geq 0$ . Equation (4) is written in units such that  $\hbar = 1$ . In the interaction representation, Eq. (4) becomes

$$i \frac{\partial}{\partial t} \begin{pmatrix} \tilde{\rho}_{11} \\ \tilde{\rho}_{12} \\ \tilde{\rho}_{21} \\ \tilde{\rho}_{22} \end{pmatrix} = \begin{pmatrix} -i\gamma_{12} & -u^* & u & i\gamma_{21} \\ -u & -i\Gamma & 0 & u \\ u^* & 0 & -i\Gamma & -u^* \\ i\gamma_{12} & u^* & -u & -i\gamma_{21} \end{pmatrix} \begin{pmatrix} \tilde{\rho}_{11} \\ \tilde{\rho}_{12} \\ \tilde{\rho}_{21} \\ \tilde{\rho}_{22} \end{pmatrix} . \quad (6)$$

Since  $\text{Tr}[\rho] = 1$ , the density matrix  $\rho$  depends on three real parameters which can be given by the coordinates of the coherence vector [42] :  $x_1 = 2\Re[\tilde{\rho}_{12}]$ ,  $x_2 = 2\Im[\tilde{\rho}_{12}]$  and

$x_3 = \tilde{\rho}_{22} - \tilde{\rho}_{11}$ . From Eq. (6), one deduces that the coordinates  $x_i$  satisfy the following system of inhomogeneous linear differential equations

$$\begin{cases} \dot{x}_1 = -\Gamma x_1 + u_2 x_3 \\ \dot{x}_2 = -\Gamma x_2 - u_1 x_3 \\ \dot{x}_3 = (\gamma_{12} - \gamma_{21}) - (\gamma_{12} + \gamma_{21})x_3 + u_1 x_2 - u_2 x_1 \end{cases}, \quad (7)$$

$u_1$  and  $u_2$  being two real functions such that  $u = u_1 + iu_2$ . As  $\text{Tr}[\rho^2] \leq 1$ , we also have  $x_1^2 + x_2^2 + x_3^2 \leq 1$  which defines the Bloch ball. The dynamics is called either unital if  $\gamma_{12} = \gamma_{21}$  i.e. the fixed point of the free dynamics is the center of the Bloch ball or affine otherwise [16, 17].

To simplify the study, we restrict the dynamics to a submanifold  $M \subset \mathbb{R}^2$  by assuming that the control field is real i.e.  $u_2 = 0$ . This hypothesis means that the control field is linearly polarized. With this choice of control, the last two equations of the system of Eqs. (7) are decoupled from the first one and the problem is reduced to  $\mathbb{R}^2$ . The system of Eqs. (7) then becomes

$$\begin{cases} \dot{x}_2 = -\Gamma x_2 - u x_3 \\ \dot{x}_3 = \gamma_- - \gamma_+ x_3 + u x_2 \end{cases}, \quad (8)$$

where  $\gamma_- = \gamma_{12} - \gamma_{21}$  and  $\gamma_+ = \gamma_{12} + \gamma_{21}$ . The coordinate  $x_1$  is set initially to 0. To simplify the notation, the index 1 of  $u_1$  has been omitted when confusion is unlikely to occur. Note that the analysis of the optimal control on  $\mathbb{R}^3$  is considerably more complex [29] and goes beyond the scope of this paper. Equations (8) can be written in a more compact form

$$\dot{\mathbf{x}} = F + uG, \quad (9)$$

with the vector  $\mathbf{x}$  of coordinates  $(x_2, x_3)$  and the two vector fields  $F$  and  $G$  defined by

$$F = \begin{pmatrix} -\Gamma x_2 \\ \gamma_- - \gamma_+ x_3 \end{pmatrix} \text{ and } G = \begin{pmatrix} -x_3 \\ x_2 \end{pmatrix}. \quad (10)$$

Finally, a straightforward calculation shows that the fixed-point of the free-dynamics is given for  $\gamma_+ \neq 0$  by

$$\begin{cases} x_2 = 0 \\ x_3 = \frac{\gamma_-}{\gamma_+} \end{cases}, \quad (11)$$

which is therefore either affine or unital according to the value of  $\gamma_-$ . The irreversibility of the dissipation effects is reflected in the fact that the vector field  $F$  is a true drift term which cannot be eliminated by unitary transformations [30].

### III. PONTRYAGIN MAXIMUM PRINCIPLE

We analyze the optimal control of this two-level system with the constraint of minimizing the total time of the control. We assume that the field  $u$  is bounded by

$$|u| \leq 1 . \quad (12)$$

Equations (8) being linear, other bounds for  $u$  can be considered from a standard rescaling of the time and the dissipative constants  $\Gamma$ ,  $\gamma_+$  and  $\gamma_-$ . The Pontryagin maximum principle [27, 28, 29, 41] is formulated from the following pseudo-Hamiltonian  $H_P$

$$H_P = \mathbf{p} \cdot (F + uG) + p_0 , \quad (13)$$

where  $\mathbf{p} = (p_2, p_3) \in (\mathbb{R}^2)^*$  is called the adjoint state and  $p_0$  is a negative constant. We recall that the cost function for the minimum time problem is equal to 1. This term is multiplied by the constant  $p_0$  in the Hamiltonian  $H_P$ . The Pontryagin maximum principle states that the extremal trajectories maximize  $H_P$  i.e.

$$H_{max}(\mathbf{x}, \mathbf{p}) = \text{Max}_{|u| \leq 1} H_P(\mathbf{x}, \mathbf{p}, u) . \quad (14)$$

The coordinates of the extremal vector state  $\mathbf{x}$  and of the corresponding adjoint state  $\mathbf{p}$  fulfill the Hamilton equations

$$\begin{cases} \dot{x}_2 = -\Gamma x_2 - u x_3 \\ \dot{x}_3 = \gamma_- - \gamma_+ x_3 + u x_2 \end{cases} , \quad (15)$$

and

$$\begin{cases} \dot{p}_2 = \Gamma p_2 - u p_3 \\ \dot{p}_3 = \gamma_+ p_3 + u p_2 \end{cases} , \quad (16)$$

where  $u$  is here the extremal control given by Eq. (14).

We can now pass to the construction of the optimal syntheses. The construction begins with the introduction of two sets of points  $\Delta_A^{-1}(0)$  and  $\Delta_B^{-1}(0)$  denoted  $C_A$  and  $C_B$  which divide  $M$  in different regions [28].  $\Delta_A$  and  $\Delta_B$  are two functions from  $M$  to  $\mathbb{R}$  defined as follows

$$\begin{cases} \Delta_A(\mathbf{x}) = \text{Det}(F, G) \\ \Delta_B(\mathbf{x}) = \text{Det}(G, [F, G]) \end{cases} , \quad (17)$$

where  $Det$  is the determinant of two vector fields and  $[\cdot, \cdot]$  their commutator. In our case, simple algebra leads to

$$\begin{cases} \Delta_A(\mathbf{x}) = -\Gamma x_2^2 + \gamma_- x_3 - \gamma_+ x_3^2 \\ \Delta_B(\mathbf{x}) = 2\Gamma x_2 x_3 - 2\gamma_+ x_2 x_3 + \gamma_- x_2 \end{cases} . \quad (18)$$

The major role of these two sets in the resolution of the optimal control problem will be detailed in Sec. V. We can already say that  $C_A$  and  $C_B$  are responsible for qualitative modifications of the optimal trajectories [28, 29]. A preliminary step thus consists in analyzing the structure of the sets  $C_A$  and  $C_B$  when  $\Gamma$ ,  $\gamma_+$  and  $\gamma_-$  vary with the conditions  $\gamma_+ \geq 0$  and  $\Gamma \geq \frac{\gamma_+}{2}$ . From a formal point of view, this can be done by introducing the feed-back group [29] but the dynamics being here bilinear [Eqs. (8)], we can directly compute the sets  $C_A$  and  $C_B$  and their relative positions.

If  $\Gamma \neq \gamma_+$  then the set  $C_B$  corresponds to the union of the two lines

$$x_2 = 0 , \quad (19)$$

and

$$x_3 = \frac{-\gamma_-}{2\Gamma - 2\gamma_+} , \quad (20)$$

with the restriction that  $|x_3| \leq 1$ . In the case  $\Gamma = \gamma_+$ ,  $C_B$  is only composed of the vertical line of equation  $x_2 = 0$ . The points  $(x_2, x_3)$  of the Bloch ball that are solutions of the polynomial equation  $\gamma_+ x_3^2 - \gamma_- x_3 - \Gamma x_2^2 = 0$  belong to  $C_A$ . In the case  $\gamma_- \neq 0$ ,  $C_A$  is therefore the union of two parabolas. This set is either above or below the line  $x_3 = \frac{-\gamma_-}{2\Gamma - 2\gamma_+}$  according to the signs of  $\gamma_-$  and of  $\Gamma - \gamma_+$ . For  $\gamma_- = 0$ , this set is reduced to the origin of the Bloch ball. Figure 1 displays the submanifold  $M$  together with the sets  $C_A$  and  $C_B$  for a given value of the parameters. We finally notice that the fixed-point of the free dynamics and the center of the Bloch ball belong to  $C_A$ .

#### IV. REACHABLE SETS AND CONTROLLABILITY

We consider four different qualitative cases of control which allow one to study several physically relevant situations :

- Case (a) : Conversion of a pure state into a mixed state with a unital Lindbladian ( $\gamma_-/\gamma_+ = 0$ ,  $\Gamma > \gamma_+ + 2$ ).

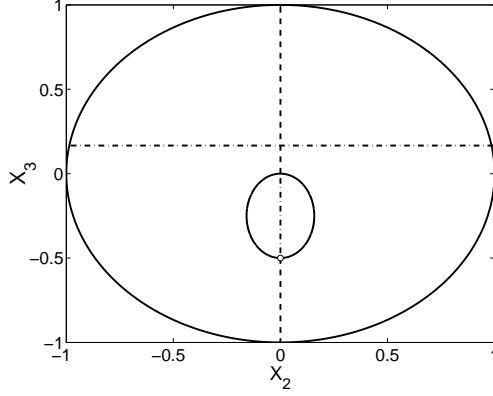


FIG. 1: Division of the manifold  $M$  by the sets  $C_A = \Delta_A^{-1}(0)$  (in solid line) and  $C_B = \Delta_B^{-1}(0)$  (in dashed and dot-dashed lines) for  $\gamma_- \neq 0$ . The dashed and dot-dashed lines represent respectively anti-turnpike and turnpike arcs which are introduced in Sec. V. The exterior circle in solid line corresponds to the limit of the Bloch ball in the plane  $(x_2, x_3)$ . The small open circle indicates the position of the fixed-point of the free-dynamics. Numerical values are taken to be  $\Gamma = 1$ ,  $\gamma_{12} = 0.1$  and  $\gamma_{21} = 0.3$ .

- Case (b) : Conversion of a pure state into a mixed state with a unital Lindbladian ( $\gamma_-/\gamma_+ = 0$ ,  $\gamma_+ - 2 < \Gamma < \gamma_+ + 2$ ).
- Case (c) : Purification of the completely random mixed state which corresponds to the center of the Bloch ball ( $\gamma_-/\gamma_+ = -1$ ,  $\Gamma > \gamma_+ + 2$ ).
- Case (d) : Conversion of a pure state into a mixed state with an affine Lindbladian ( $\gamma_-/\gamma_+ = -0.5$ ,  $\Gamma > \gamma_+ + 2$ ).

The numerical values we have chosen for illustrations are given in Table I. Although the

TABLE I: Numerical values of the dissipative constants in arbitrary units.

	$\Gamma$	$\gamma_{12}$	$\gamma_{21}$
(a)	3	0.3	0.3
(b)	1.5	0.3	0.3
(c)	3	0	1
(d)	3	0.1	0.3



choice of the parameters of Table I will become clearer in Sec. V, some comments can already be made. This choice both depends on the structure of the sets  $C_A$  and  $C_B$  and on the characteristics of two particular extremals denoted  $X-$  and  $Y-$  which start at the initial point, and correspond respectively to a constant control equal to -1 and 1. As detailed in the appendix B, the  $X-$  and  $Y-$  trajectories are either pseudo-periodic or aperiodic according to the sign of the discriminant  $\Delta = (\Gamma - \gamma_+)^2 - 4$  of the system of Eqs. (8). An exact resolution of the dynamics shows that the trajectory of the system is aperiodic if  $\Delta > 0$  and pseudo-periodic otherwise. This point is summarized by the diagram 10 of the appendix B. In Table I, we have chosen for three of the four examples  $\Gamma$  such that  $\Gamma > \gamma_+ + 2$  to simplify the local structure of the optimal synthesis around the fixed-point of the dynamics. A pseudo-periodic trajectory is locally a spiral in the plane  $(x_2, x_3)$  around this fixed point which makes the analysis more complex (see Sec. V).

### A. Purity and limits of the dynamics

Before analyzing the reachable set and the controllability of each example, we begin by some general comments about the dynamics.

We first show that the field cannot locally compensate the effect of dissipation. The purity of the quantum state is defined by the function  $2\text{Tr}[\rho^2] - 1 = x_2^2 + x_3^2$ . Pure states are thus on the unit circle of the  $(x_2, x_3)$  plane. Simple algebra then leads to

$$\frac{d(\text{Tr}[\rho^2])}{dt} = -\Gamma x_2^2 + \gamma_- x_3 - \gamma_+ x_3^2, \quad (21)$$

and we notice that this derivative does not depend on  $u$ , which completes the proof. A more general proof of this point is given in Refs. [16, 17]. We also point out that for points  $\mathbf{x}$  where  $\Delta_A(\mathbf{x}) < 0$  then  $\frac{d\text{Tr}[\rho^2]}{dt} < 0$  and inversely if  $\Delta_A(\mathbf{x}) > 0$  then  $\frac{d\text{Tr}[\rho^2]}{dt} > 0$ . The curve  $C_A$  divides the plane  $(x_2, x_3)$  into a region where the purity of the state locally increases and a region where it locally decreases. On the boundary  $C_A$ , the purity is preserved. This point can be qualitatively understood as follows. We recall that the purity is equal to the square of the distance to the origin. The conservative vector field  $G$  is orthoradial (i.e. normal to radial vectors) for each point  $(x_2, x_3) \neq (0, 0)$  of the manifold. The dissipative vector field  $F$  does not modify the purity of the state if the radial component of  $F$  vanishes i.e. if  $F$  is parallel to  $G$  which is the definition of the curve  $C_A$ .

We next analyze the fixed points of the dynamics when the field is on, which are defined by  $F + uG = 0$ . Since  $F$  and  $G$  are parallel, the fixed points belong to the curve  $C_A$ . The field-free limit point is the point of this line of maximum purity (see for instance Fig. 1). This shows that the dissipation alone allows to reach the state of maximum purity. Inversely, one can ask if every point of the curve  $C_A$  corresponds to a limit point of the dynamics. The answer is positive for a real non-bounded control  $u$  since the limits can be written

$$\begin{cases} x_2 = \frac{-u\gamma_-}{\Gamma\gamma_+ + u^2} \\ x_3 = \frac{\gamma_-}{\gamma_+ + u^2/\Gamma} \end{cases} . \quad (22)$$

## B. Reachable sets

We begin by recalling some results of Refs. [16, 17] about controllability of dissipative systems. A quantum dissipative system of finite dimension whose dynamics is governed by the Lindblad equation is generically accessible but not controllable. The accessibility property characterizes the fact that the system can be driven in every direction of the state space. Moreover, the concept of accessibility does not take into account the reversibility or the irreversibility of the process. The lack of controllability is measured by the non small-time controllability of the system which illustrates the irreversibility of the dynamics. This kind of system is not small-time controllable because the field cannot locally compensate the effect of dissipation as shown by Eq. (21). The accessibility property can be checked by the computation of the dimension of the dynamical Lie algebra  $L$  of the system [16, 17]. We introduce for that purpose the density matrix  $\bar{\rho}$  of coordinates  $(1, x_2, x_3)$  which is given in the basis of the coherence vector and we rewrite Eqs. (8) in matrix form as follows

$$\dot{\bar{\rho}} = \mathcal{L}_F \bar{\rho} + u \mathcal{L}_G \bar{\rho} , \quad (23)$$

where  $\mathcal{L}_F$  and  $\mathcal{L}_G$  are  $3 \times 3$  matrices given by

$$\mathcal{L}_F = \begin{pmatrix} 0 & 0 & 0 \\ 0 & -\Gamma & 0 \\ \gamma_- & 0 & -\gamma_+ \end{pmatrix} \text{ and } \mathcal{L}_G = \begin{pmatrix} 0 & 0 & 0 \\ 0 & 0 & -1 \\ 0 & 1 & 0 \end{pmatrix} . \quad (24)$$

$L$  is the Lie algebra generated by  $\mathcal{L}_F$  and  $\mathcal{L}_G$ . If  $\Gamma \neq \gamma_+$ , a direct computation shows that  $L$  is either isomorphic to  $\mathfrak{gl}(2)$  or to the semi-direct sum  $\mathfrak{gl}(2) \ltimes \mathbb{R}^2$  of respective dimensions

4 and 6 for  $\gamma_- = 0$  or  $\gamma_- \neq 0$ . The system is therefore accessible for  $\Gamma \neq \gamma_+$ .

We now determine the reachable sets from their respective initial states of the four examples. The reachable sets can be constructed by the explicit construction of all the trajectories. We denote by  $\mathcal{R}(\mathbf{x}_0)$  the reachable set from  $\mathbf{x}_0$ . We first search for in this section the boundary of the reachable sets. Then in Sec. V we show that all the points inside the boundary are attainable. We consider for that the  $X-$  and  $Y-$  trajectories starting from the initial point and from the field-free fixed point of the dynamics. A qualitative change occurs when the  $X-$  or  $Y-$  trajectories cross  $C_A$  since the angle between the vector  $F(\mathbf{x})$  and  $G(\mathbf{x})$  changes its sign. The determination of all the extremal trajectories in Sec. V allows us to complete the construction.

We apply these remarks to the cases (a) and (b) where the initial point has coordinates  $(x_2 = 0, x_3 = 1)$  and  $C_A$  is reduced to the origin  $(x_2 = 0, x_3 = 0)$ . The origin is attained asymptotically by the dynamics when  $t \rightarrow +\infty$ . The  $Y-$  and  $X-$  trajectories, which have the same initial and final points, are therefore global boundaries of the reachable set. This point is illustrated in Figs. 2a and 2b for the cases (a) and (b), where the reachable set  $\mathcal{R}$  is in grey.

For the case (c), the  $X-$  and  $Y-$  trajectories starting from  $(x_2 = 0, x_3 = 0)$  intersect asymptotically  $C_A$ . We also consider the  $X-$  and  $Y-$  trajectories starting from the field-free fixed point which define two new regions. As an infinite time is necessary to reach this point, these two trajectories do not belong to the reachable set.  $\mathcal{R}$  is the union of all these regions as shown in Fig. 2c. We will check in Sec. V by constructing the extremal trajectories that every point of this set is effectively attainable.

For the case (d) the situation is more difficult to analyze as the  $X-$  and  $Y-$  trajectories starting from  $(x_2 = 0, x_3 = 1)$  intersect transversally  $C_A$ . From this point of intersection, the two trajectories do not correspond anymore to the boundary of  $\mathcal{R}$ . After the crossing of  $C_A$ , the  $X-$  or  $Y-$  trajectories originating from the preceding curves define two new regions of  $\mathcal{R}$ . We finally consider the limit point of the field-free dynamics which can be attained as  $t \rightarrow +\infty$  and the  $X-$  and  $Y-$  trajectories starting from this point. These two lines define two new boundaries which intersect asymptotically  $C_A$  but which do not belong to  $\mathcal{R}$ .  $\mathcal{R}$  is therefore composed of all the regions constructed above and is displayed in Fig. 2d. As before, only the determination of the extremal trajectories will complete the construction.

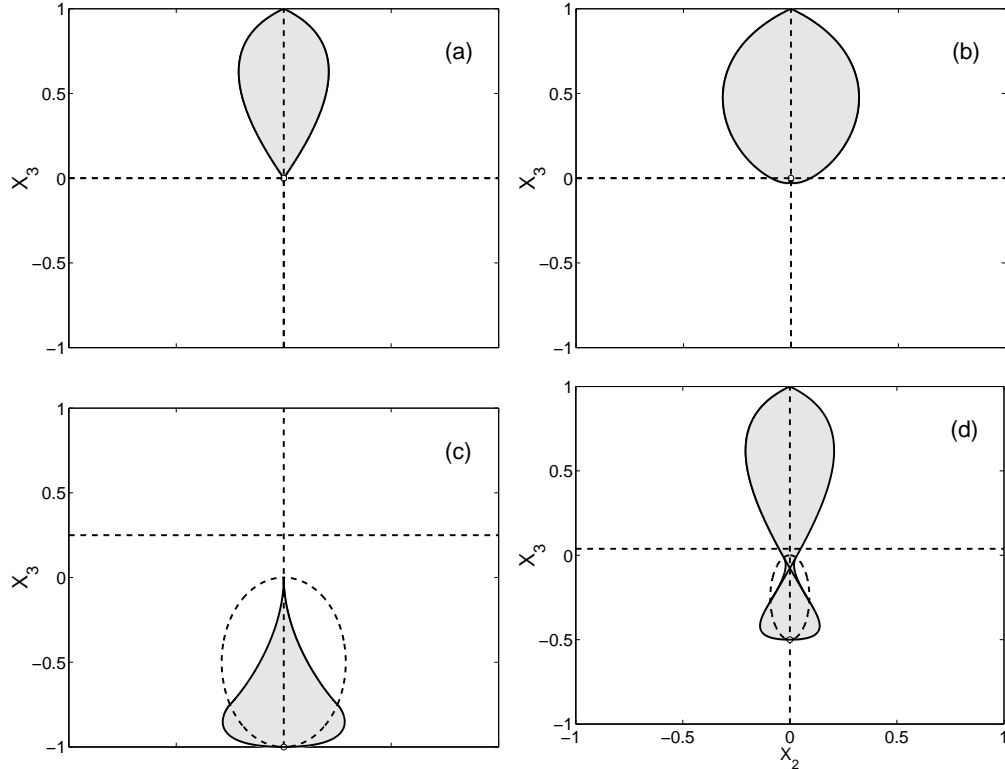


FIG. 2: Reachable sets  $\mathcal{R}$  (in grey) for the cases (a), (b), (c) and (d). The sets  $C_A$  and  $C_B$  are represented in dashed lines. The position of the field-free fixed point is indicated by the small open circle. In (c) and (d), the trajectories starting from the field-free fixed point do not belong to  $\mathcal{R}$  (see text).

## V. TIME-OPTIMAL CONTROL

The application of the Pontryagin maximum principle is particularly simple at least locally in the case of time minimum control. The goal of this section is to solve this problem by constructing the optimal synthesis i.e. the set of all the optimal solutions starting from a given initial point  $\mathbf{x}_0$  and reaching a point of  $\mathcal{R}(\mathbf{x}_0)$ . For time optimization, the optimal controls are composed of piecewise constant parts ( $u = \pm 1$ ) and of singular controls. Some preliminary work in Sec. V A has to be done before determining the optimal solutions.

## A. Preliminary

We define two functions  $\Phi$  and  $\theta$  [28].  $\Phi$ , called the switching function, is given by

$$\Phi(t) = \mathbf{p}.G = -p_2x_3 + p_3x_2 . \quad (25)$$

Using Eq. (13), standard considerations of maximization of the pseudo-Hamiltonian  $H_P$  lead to the conclusion that the extremal field at time  $t$  is given by  $u = \text{sign}(\Phi(t))$  if  $\Phi(t) \neq 0$ . A time  $t_0$  such that the control changes sign (i.e. such that  $\Phi(t_0) = 0$ ) is a switching time. If  $\Phi$  vanishes on an interval  $[t_0, t_1]$  then the corresponding trajectory is called singular and is referred to as a  $Z$ -trajectory. An important point is the fact that the  $Z$ -trajectories lie in the set  $C_B$  and that the corresponding control  $u = \phi$  is singular i.e. different from 1 or -1.  $\phi$  can be calculated by imposing that  $\frac{d}{dt}\Delta_B(\mathbf{x}(t)) = 0$  on  $[t_0, t_1]$ . In our case, it can be shown that

$$\frac{d}{dt}\Delta_B(\mathbf{x}(t)) = 0 = \frac{\partial\Delta_B}{\partial x_2}x_2 + \frac{\partial\Delta_B}{\partial x_3}x_3 . \quad (26)$$

One arrives after simple algebra to

$$\phi(\mathbf{x}) = \frac{-x_2\gamma_-(\Gamma - 2\gamma_+) - 2x_2x_3(\gamma_+^2 - \Gamma^2)}{2(\Gamma - \gamma_+)(x_2^2 - x_3^2) - \gamma_-x_3} . \quad (27)$$

For the line  $x_2 = 0$  of  $C_B$ , this leads to  $\phi(\mathbf{x}) = 0$ . For the line  $x_3 = \frac{-\gamma_-}{2(\Gamma - \gamma_+)}$ , we obtain

$$\phi(\mathbf{x}) = \frac{\gamma_-(\gamma_+ - 2\Gamma)}{2(\Gamma - \gamma_+)x_2} . \quad (28)$$

The control is admissible if  $|\phi(\mathbf{x})| \leq 1$  which implies here the condition

$$|x_2| \geq \left| \frac{\gamma_-(\gamma_+ - 2\Gamma)}{2(\Gamma - \gamma_+)} \right| . \quad (29)$$

Not every  $Z$ -trajectory can be an optimal trajectory. We introduce to characterize this point the notion of turnpike and anti-turnpike curves [28]. Let  $\mathbf{x} \notin C_A \cup C_B$  and the function  $f(\mathbf{x}) = -\frac{\Delta_B(\mathbf{x})}{\Delta_A(\mathbf{x})}$ . A turnpike curve is an arc lying in  $C_B$  such that for every point  $\mathbf{x}$  of this arc  $\Delta_A(\mathbf{x}) \neq 0$  and  $X(\mathbf{x})$  and  $Y(\mathbf{x})$  are not tangent to  $C_B$ . It is also assumed that  $X(\mathbf{x})$  and  $Y(\mathbf{x})$  point to opposite sides of  $C_B$  which define two regions  $\Omega_x$  and  $\Omega_y$ . If  $f(\mathbf{x}) > 0$  (resp.  $f(\mathbf{x}) < 0$ ) on  $\Omega_y$  and  $f(\mathbf{x}) < 0$  (resp.  $f(\mathbf{x}) > 0$ ) on  $\Omega_x$  then the arc is a turnpike (resp. anti-turnpike) arc. The relation with the optimal synthesis can be stated as follows. Using for instance the clock form  $\alpha$  (see appendix A), it can be shown that the anti-turnpike trajectories are not optimal. Figure 1 displays the turnpike and the anti-turnpike

curves for particular values of the parameters.

The switching function  $\Phi$  is a powerful tool that gives all the informations on the extremal trajectory. However, a global analysis of the extremals using only  $\Phi$  is difficult because all the initial values  $(p_{20}, p_{30})$  have to be tested. A more global point of view is given by the function  $\theta$  which has the advantage not to depend on  $\mathbf{p}$ .

Let  $\mathbf{v}$  be the vector of coordinates  $(x_2, x_3)$ . Deriving Eqs. (8) with respect to time, it can be shown that  $\mathbf{v}$  satisfies the following system of equations

$$\begin{cases} \dot{v}_2 = -\Gamma v_2 - uv_3 \\ \dot{v}_3 = -\gamma_+ v_3 + uv_2 \end{cases} . \quad (30)$$

We next introduce the vector  $\tilde{v}(t)$ . At time  $t$ , let us assume that the dynamics reaches the point  $(x_2(t), x_3(t))$  and that the vector field  $G$  at this point is given by  $G(x_2(t), x_3(t)) = G(t)$ .  $\tilde{v}(t)$  is defined as the solution at time 0 of Eqs. (30) that at time  $t$  is equal to  $G(t)$ . The dynamics is thus propagated backwards during the time  $t$ .  $\theta$  is then defined as

$$\theta(t) = \arg(\tilde{v}(0), \tilde{v}(t)) , \quad (31)$$

where the angle is measured counterclockwise. The definition of  $\theta$  originates from the fact that the product  $\mathbf{p}(t) \cdot \mathbf{v}(t)$  is a constant [28]. We thus have

$$\Phi(t) = p(t) \cdot G(t) = p(0) \cdot \tilde{v}(t) . \quad (32)$$

The function  $\theta$  allows to determine some properties of the extremal trajectories. We briefly recall these points here. The reader is referred to [28] for rigorous definitions and complete proofs. It can first be shown that

$$\text{sign}(\dot{\theta}) = \text{sign}(\Delta_B) , \quad (33)$$

which means that the zeros of  $\dot{\theta}$  are located on  $C_B$ . A switch can occur if  $\dot{\theta} > 0$  and  $\theta > 0$  or  $\dot{\theta} < 0$  and  $\theta < 0$ . In addition, the variation of  $\theta$  between two switches or between a switch and a singular control is equal to 0 modulo  $\pi$ . This latter point can be easily understood from Eq. (32). Other properties of  $\theta$  will be detailed during the construction of the optimal synthesis.

## B. Time-optimal syntheses

The parts VB1, VB2, VB3 and VB4 are rather technical and describe the way to obtain the optimal syntheses. Section VB5 details conclusions on the role of the dissipation that can be gained from the resolution of the time optimal control.

### 1. Case (a)

In the case (a), the optimal trajectories are either bang or bang-bang. A bang trajectory is a trajectory associated to a single value of the control  $u = +1$  or  $u = -1$ . A bang-bang trajectory is the concatenation of an  $X-$  and an  $Y-$  trajectories. We denote by  $X * Y$  such a concatenation where the  $Y-$  trajectory comes first. Here the maximum number of switches is thus equal to 1. The elimination of extremal trajectories selected by the Pontryagin maximum principle has been done through the clock form  $\alpha$  (see appendix A for details) and the symmetry of the diagram with respect to the line  $x_2 = 0$ . We recall that the clock form can only be used for trajectories belonging to one of the four quadrants defined by  $C_B$  and which do not cross  $C_A$ . Figure 3 displays the optimal synthesis for this problem and the evolution of the angle  $\theta$  along the  $Y-$  trajectory starting from the initial point  $(0, 1)$ . The plot of  $\theta$  shows that the switches are always permitted along the  $X-$  or the  $Y-$  trajectory. Note also that the form of the curve representing  $\theta$  is related to the sign of  $\Delta$ . More precisely, if  $\Gamma > \gamma_+ + 2$  then  $\theta$  is a monotonically decreasing function and if  $\Gamma < \gamma_+ - 2$  (case not treated here),  $\theta$  starts increasing, passes through a maximum when the trajectory crosses  $C_B$  and then decreases. The intermediate case  $\gamma_+ - 2 < \Gamma < \gamma_+ + 2$  corresponds to the case (b). Using the clock form, it can be shown that only one switch is possible for a trajectory in a given quadrant. This point can also be determined from more general considerations detailed in Ref. [28]. The rest of the optimal synthesis is deduced from the symmetry of the problem. The line  $x_2 = 0$  is called an overlap curve denoted by  $K$  as it is the locus of points reached by two optimal trajectories. We finally notice that the dissipation alone is not used here by the control and therefore cannot help accelerating the control. We recall that the singular control on the vertical line of  $C_B$  is given by  $u = 0$ .

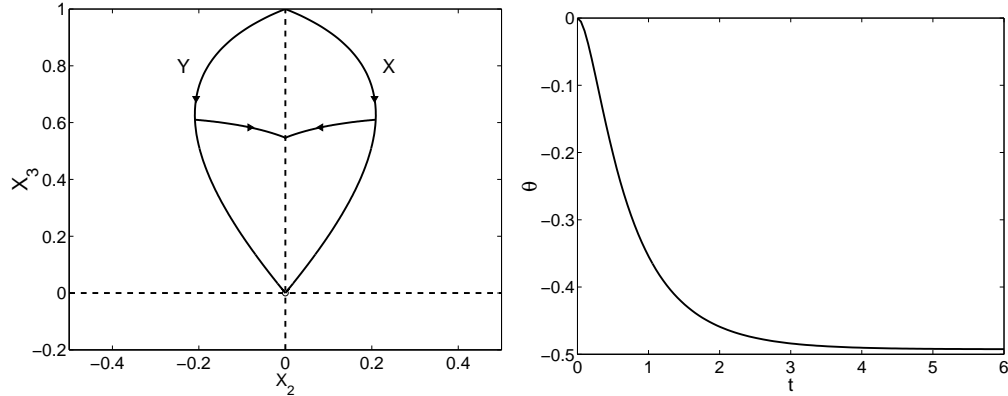


FIG. 3: The top figure represents the optimal synthesis for the case (a) (see text). The dashed lines indicate the locus  $C_B$  and the small open circle the fixed point of the dynamics. The bottom figure displays the evolution of  $\theta$  as a function of the time for the  $Y$ - trajectory starting from the point  $(0,1)$ .

## 2. Case (b)

The situation is a little more complex in the case (b). For  $x_3 > 0$ , the synthesis is similar to the one of case (a) i.e. the trajectories are either bang or bang-bang. The function  $\theta$  is here periodic, the times where  $\dot{\theta}$  vanishes correspond to the crossing of  $C_B$ . This function tells also us that the initial  $Y$ - and  $X$ - trajectories cannot switch in their respective second quadrant (i.e. the second quadrant they go through) since  $\dot{\theta}(t) > 0$  and  $\theta(t) < 0$ . By symmetry with respect to the line  $x_2 = 0$ , one deduces that these curves are optimal up to this line. A singular control along the horizontal line of  $C_B$  is optimal from the point of intersection between the initial  $X$ - or  $Y$ - trajectories and this line. Since  $\gamma_- = 0$ , the singular control is given by  $\phi = 0$ . From this singular line originate optimal trajectories with control  $u = \pm 1$ . Using the clock form  $\alpha$ , it can be shown that these trajectories can not switch again. To summarize, in this second part we have constructed optimal controls of the form  $Y * Z * X$ ,  $Y * Z * Y$ ,  $X * Z * X$  and  $X * Z * Y$ . This optimal synthesis is represented in Fig. 4. Here, one sees that the dissipation alone (with  $u = 0$ ) accelerates the control to reach a point near the origin only along the horizontal direction and for  $x_3 = 0$ . We finally give in Fig. 5 an example of the comparison of two extremal trajectories. The time to reach respectively the points A and B from the initial point  $(0,1)$  by the  $Y$ - and  $X$ - trajectories is the same. We would like to attain the point C from A or B. We use



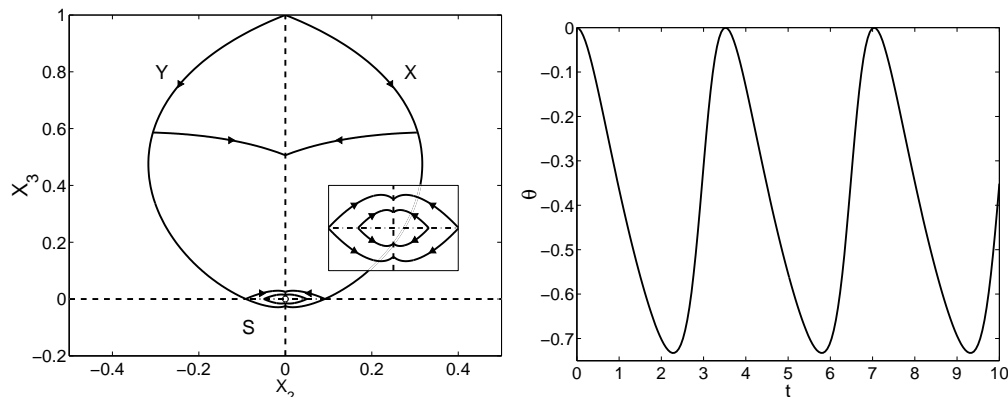


FIG. 4: Same as Fig. 3 but for the case (b). The dotted-dashed line represents the singular trajectory  $S$ . The small insert is a zoom of the optimal synthesis near the origin.

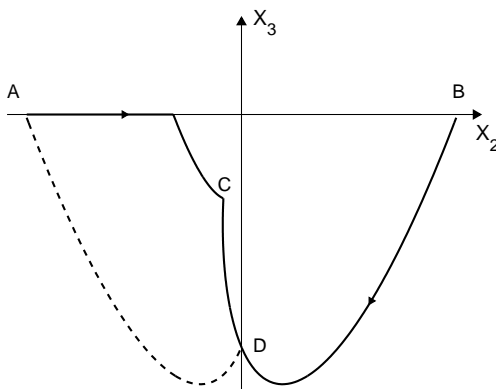


FIG. 5: Use of symmetry to determine the optimal trajectory (see text).

either the  $X$ -trajectory from B or a concatenation of a  $Y$ - and a  $Z$ - ones from A. The clock form  $\alpha$  cannot be used here since the trajectories belong to two different quadrants. We therefore consider the symmetric image AD of the curve BD with respect to  $x_2 = 0$ . The two extremals are thus in the same quadrant and  $\alpha$  can be used. We conclude that the curve  $Y * Z * Y$  is optimal to reach the point  $C$ .

### 3. Case (c)

In this case, the singular line  $x_2 = 0$  is optimal. The singular control is equal to zero. Switches can occur from the initial  $X$ - and  $Y$ - trajectories but they do not lead to optimal trajectories. Inversely,  $X$ - and  $Y$ - trajectories originating from  $S$  are found to be optimal. When two extremals cross  $C_A$ ,  $\alpha$  cannot be used and a direct numerical comparison is then

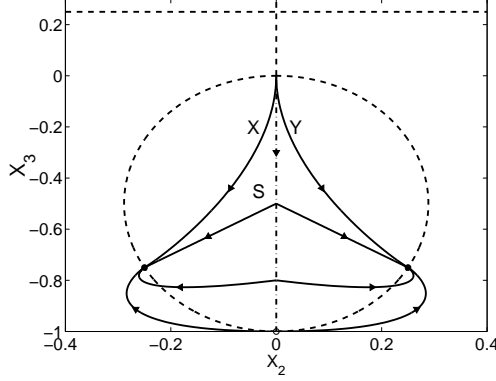


FIG. 6: Same as Fig. 4 but for the case (c).

performed. In this case, the function  $\theta$  tells us that these curves do not switch. Trajectories originating from  $S$  that have a switch are therefore not extremal. We finally point out that the dissipation is beneficial for the control and decreases the duration needed to purify the system. The optimal controls are here of the form  $X-$ ,  $Y-$ ,  $X * Z$  or  $Y * Z$ . Figure 6 displays the optimal synthesis for this problem.

#### 4. Case (d)

The case (d) is the more complex one and corresponds roughly to the composition of cases (b) and (c). The difficulty lies in the global structure of the control or, in other words, in gluing the two preceding local analysis. For  $x_3 > 0$ , the optimal synthesis is similar to the cases (a) or (b) with bang or bang-bang trajectories. The bottom of the optimal synthesis from the point of intersection of the initial  $X-$  and  $Y-$  trajectories is similar to the case (c).

We now describe the central part of the synthesis. The horizontal singular line of  $C_B$  does not correspond to a singular trajectory since  $|\phi(\mathbf{x})| > 1$  which is a non-admissible control. Consider the first point of intersection of  $C_B$  with the  $X-$  or  $Y-$  trajectory. Following [28], we know that a switch curve  $C$  originates from this point. To determine the exact locus of  $C$ , we use the  $\theta$  function since this function varies by 0 modulo  $\pi$  between two switches.  $C$  is constructed numerically. By definition of  $C$ , every trajectory which crosses  $C$  switches on  $C$ . We have found that  $C$ ,  $C_B$  and  $C_A$  intersect in one point, the origin  $O$ .

Since the line  $x_2 = 0$  is turnpike for  $\frac{\gamma_-}{\gamma_+} < x_3 < 0$ , we can ask if this singular trajectory is

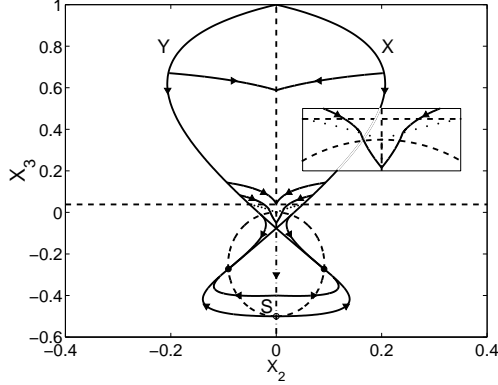


FIG. 7: Same as Fig. 4 but for the case (d). The dotted line represents the switch curve  $C$ .

optimal i.e. if we can have a local optimal synthesis of the form given by Fig. 8. To answer this question, we use the switching function  $\Phi$ . For  $\mathbf{x}(t) \in C \cup S$ ,  $\Phi(t) = 0$  i.e. the vectors  $\mathbf{p}(t)$  and  $G(\mathbf{x}(t))$  are orthogonal. Since the direction of  $G$  is known ( $G$  is orthoradial), one can deduce the direction of  $\mathbf{p}(t)$ . Let  $\mathbf{z}_1$  and  $\mathbf{z}_2$  be two points belonging respectively to  $C$  and  $S$ . The vectors  $G(\mathbf{z})$  associated to these points are schematically represented in Fig. 8. We let now the states  $\mathbf{z}_1$  and  $\mathbf{z}_2$  go to  $(0, 0)$  and we determine the directions of the different adjoint states. We recall that the Pontryagin maximum principle states that  $\mathbf{p}$  is a continuous function which does not vanish. When  $\mathbf{z}_1$  goes to  $(0, 0)$ , one deduces by a continuity argument that  $\mathbf{p}_1$  is vertical in  $O$ . When  $\mathbf{z}_2$  goes to  $(0, 0)$ , the limit direction of  $\mathbf{p}_2$  is given by the switch curve  $C$ . To respect the continuity of  $\mathbf{p}$ , one sees that  $C$  has to be tangent to the line  $x_2 = 0$  in  $O$ . Due to the complexity of analytical calculations, we have checked numerically that this is not the case. The singular line for  $x_3 < 0$  is therefore not optimal. The trajectories of the form  $Y * X * Y$  or  $X * Y * X$  are thus optimal up to  $x_2 = 0$ . In addition, when the initial  $X$ - and  $Y$ - trajectories cross  $C_A$ , the angle between the vectors  $F(\mathbf{x})$  and  $G(\mathbf{x})$  changes its sign. New optimal trajectories originate from this point of intersection and correspond to two new regions of the reachable set.

##### 5. Qualitative conclusions on the dynamics

From the results obtained in the preceding sections, some qualitative conclusions can be made with respect to the dissipation effect on the time optimal control of the dynamics. The dissipation is not undesirable when the dissipation allows to purify the system [cases

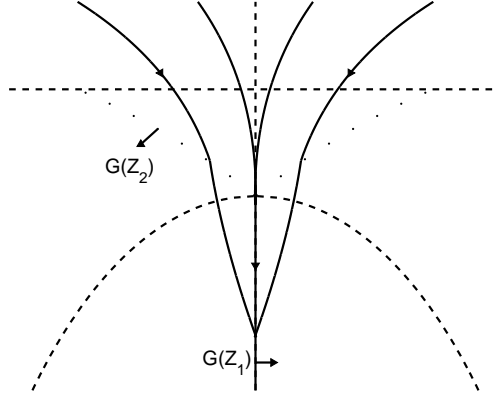


FIG. 8: Possible optimal synthesis around the origin.

(c) and (d)] and help accelerating the control. In contrast for the conversion of a pure state into a mixed state, the dissipation alone increases the duration of the control and its effect is not beneficial for the control [cases (a) and (b)]. The example (d) summarizes well the situation. As long as the purity of the state decreases, it is advantageous to use a control field but when the purity starts increasing the dissipation alone becomes more efficient.

Finally, we point out that a visual inspection of the optimal syntheses allows to check the form of the reachable sets given in Sec. IV B.

## VI. CONCLUSION

We have investigated the time-optimal control of a two-level dissipative system. For different initial and final points, we have constructed the optimal syntheses which allow us to rigorously conclude on the beneficial role of the dissipation in order to reduce the duration of the process. An open question is the generalization of the present study to more complex quantum systems with for instance two control parameters or three levels. The determination of the optimal syntheses for these systems requires more sophisticated mathematical tools than those used in this paper [29]. In addition, such an analysis could also be performed on other problems of quantum control. We point out that the question of measurement in the context of geometrical control theory is particularly interesting. Measurements can be viewed as a non-unitary control which allows to enlarge the reachable sets. For instance, we can consider systems not completely controllable by unitary control but which become controllable if measurements are used. A simple example is given by a finite number of

levels of the harmonic oscillator with a constant dipolar interaction only between adjacent energy levels [43]. From a formal point of view, this problem raises the challenge of the precise formulation of the Pontryagin maximum principle in this context which is to our knowledge an open question. We notice that all these geometrical tools would allow us to answer some physical relevant questions such as the time at which measurements have to be done to minimize the duration of the control.

## APPENDIX A: THE CLOCK FORM

We derive in this section the expression of the clock form denoted  $\alpha$  [29]. By definition, the clock form is a 1-form which fulfills the following conditions

$$\begin{cases} \alpha(F) = 1 \\ \alpha(G) = 0 \end{cases} . \quad (\text{A1})$$

A solution of this system exists except on the set  $C_A$  where  $F$  and  $G$  are collinear. If we write  $\alpha$  as  $\alpha = \alpha_2 dx_2 + \alpha_3 dx_3$  then simple algebra shows that  $\alpha_2$  and  $\alpha_3$  are solutions of the system

$$\begin{cases} \alpha_2(-\Gamma x_2) + \alpha_3(\gamma_- - \gamma_+ x_3) = 1 \\ \alpha_2 x_3 = \alpha_3 x_2 \end{cases} . \quad (\text{A2})$$

We obtain that

$$\begin{cases} \alpha_2 = \frac{-x_2}{\Gamma x_2^2 - \gamma_- x_3 + \gamma_+ x_3^2} \\ \alpha_3 = \frac{-x_3}{\Gamma x_2^2 - \gamma_- x_3 + \gamma_+ x_3^2} \end{cases} . \quad (\text{A3})$$

From the 1-form  $\alpha$ , we can define the 2-form  $d\alpha$  which is given by

$$d\alpha = \left( \frac{\partial \alpha_3}{\partial x_2} - \frac{\partial \alpha_2}{\partial x_3} \right) dx_2 \wedge dx_3 , \quad (\text{A4})$$

and reads after some calculations

$$d\alpha = \frac{2\Gamma x_2 x_3 + \gamma_- x_2 - 2\gamma_+ x_2 x_3}{[\Gamma x_2^2 - \gamma_- x_3 + \gamma_+ x_3^2]^2} dx_2 \wedge dx_3 . \quad (\text{A5})$$

If we write  $d\alpha$  as  $d\alpha = g(x_2, x_3) dx_2 \wedge dx_3$  then one sees that  $g(x_2, x_3) = 0$  on  $C_B$  and that the function  $g$  has a constant sign in the regions delimited by the lines of  $C_B$ . This point is displayed in Fig. 9. As suggested by its name, the clock form is a form which allows one to

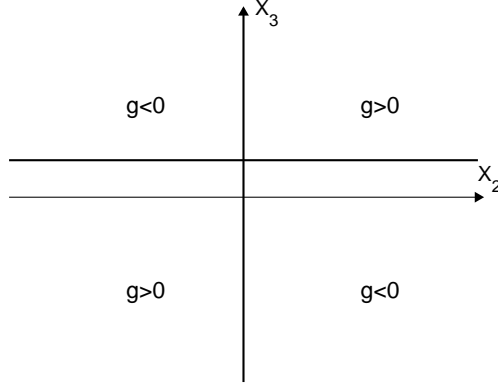


FIG. 9: Sign of the function  $g$  in the plane  $(x_2, x_3)$ . The large solid lines indicate the position of the set  $C_B$ .

determine the time taken to travel a path and to compare the extremals. Let  $\gamma$  be a path in the plane  $(x_2, x_3)$  which does not cross  $C_A$  and  $T$  the time of travel along  $\gamma$ . We have

$$\int_{\gamma} \alpha = \int_0^T \alpha(\dot{\mathbf{x}}) dt = \int_0^T \alpha(F) dt = T . \quad (\text{A6})$$

We consider now two paths  $\gamma_1$  and  $\gamma_2$  starting and ending at the same points and respectively associated to the durations  $T_1$  and  $T_2$ . One shows by using the Stokes theorem that

$$T_1 - T_2 = \int_{\gamma_1} \alpha - \int_{\gamma_2} \alpha = \int_D d\alpha , \quad (\text{A7})$$

where  $D$  is the surface delimited by  $\gamma_1 \cup -\gamma_2$ . For paths  $\gamma_1$  and  $\gamma_2$  which lie in one of the four quadrants defined by  $C_B$ , we can straightforwardly determine the time-optimal trajectory.

## APPENDIX B: ANALYTICAL DETERMINATION OF THE DYNAMICS

In this section, we solve analytically the dynamics of the system given by the following system of differential equations

$$\begin{cases} \dot{x}_2 = -\Gamma x_2 - u x_3 \\ \dot{x}_3 = \gamma_- - \gamma_+ x_3 + u x_2 \end{cases} . \quad (\text{B1})$$

We assume that  $u = \pm 1$  and we denote by  $u = \varepsilon$  the control term. Combining Eqs. (B1), one arrives to equations that depend on only one variable  $x_2$  or  $x_3$

$$\begin{cases} \ddot{x}_2 + (\Gamma + \gamma_+) \dot{x}_2 + (1 + \Gamma \gamma_+) x_2 + \varepsilon \gamma_- = 0 \\ \ddot{x}_3 + (\Gamma + \gamma_+) \dot{x}_3 + (1 + \Gamma \gamma_+) x_3 - \Gamma \gamma_- = 0 \end{cases} . \quad (\text{B2})$$

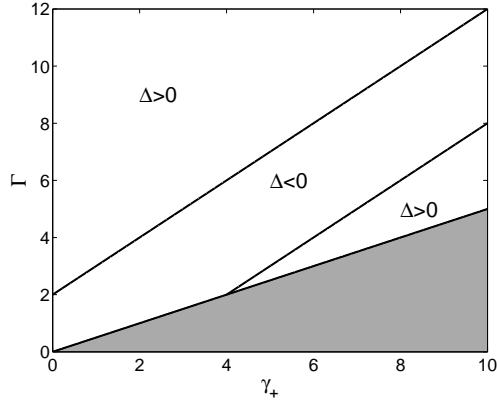


FIG. 10: Sign of the discriminant  $\Delta$  as a function of the parameters  $\Gamma$  and  $\gamma_+$ . The parameters are in arbitrary units. The zone in grey is excluded for Lindblad dynamics.

Equations (B2) are linear inhomogeneous differential equations of second order whose discriminant  $\Delta$  is given by

$$\Delta = (\Gamma - \gamma_+)^2 - 4. \quad (\text{B3})$$

A qualitative change of the solutions is expected according to the sign of  $\Delta$ , i.e. a transition from a pseudo-periodic solution for  $\Delta < 0$  to an aperiodic solution for  $\Delta \geq 0$ . This point is summarized in Fig. 10. Note that the parameter  $\gamma_-$  plays no role in the structure of these trajectories but modifies their limits points. Simple algebra allows one to calculate the exact solutions. For instance for  $\Delta > 0$ , we obtain

$$\begin{cases} x_2(t) = e^{-(\Gamma+\gamma_+)t/2} [x_{20} \cosh(\frac{\delta}{2}t) - (x_{20} \frac{\Gamma}{\delta} - x_{20} \frac{\gamma_+}{\delta} + \frac{2\varepsilon}{\delta} x_{30}) \sinh(\frac{\delta}{2}t)] \\ x_3(t) = e^{-(\Gamma+\gamma_+)t/2} [x_{30} \cosh(\frac{\delta}{2}t) + (\frac{(\Gamma-\gamma_+)}{\delta} x_{30} + \frac{2\varepsilon}{\delta} x_{20} + \frac{2\gamma_-}{\delta}) \sinh(\frac{\delta}{2}t)] \end{cases}. \quad (\text{B4})$$

where  $(x_{20}, x_{30})$  is the initial point of the dynamics and  $\delta = \sqrt{\Delta}$ .

## ACKNOWLEDGMENTS

The authors thank B. Bonnard and U. Boscaïn for many helpful discussions.

- 
- [1] W. Warren, H. Rabitz, and M. Dahleb, *Science* **259**, 1581 (1993).
  - [2] H. Rabitz, R. de Vivie-Riedle, M. Motzkus, and K. Kompa, *Science* **288**, 824 (2000).

- [3] D. Sugny, C. Kontz, M. Ndong, Y. Justum, G. Dives, and M. Desouter-Lecomte, *Phys. Rev. A* **74**, 043419 (2006).
- [4] M. A. Nielsen and I. L. Chuang, *Quantum Computation and Quantum Information* (Cambridge University Press, Cambridge, 2000).
- [5] D. Bacon, A. M. Childs, I. L. Chuang, J. Kempe, D. W. Leung, and X. Zhou, *Phys. Rev. A* **64**, 062302 (2001).
- [6] S. Lloyd and L. Viola, *Phys. Rev. A* **65**, 010101 (2002).
- [7] A. I. Solomon and S. G. Schirmer, *Group 24 : Physical and Mathematical Aspects of Symmetry*, Institute of Physics Conference **173**, 485 (2003).
- [8] J. Gong and S. A. Rice, *J. Chem. Phys.* **120**, 9984 (2004).
- [9] L. R. G. A. Olivares-Rentería, *Phys. Rev. A* **73**, 062327 (2006).
- [10] L. Roa, A. Delgado, M. L. L. de Guevara, and A. B. Klimov, *Phys. Rev. A* **73**, 012322 (2006).
- [11] A. Pechen, N. Il'in, F. Shuang, and H. Rabitz, *Phys. Rev. A* **74**, 052102 (2006).
- [12] M. Sugawara, *J. Chem. Phys.* **123**, 204115 (2005).
- [13] F. Shuang, A. Pechen, T.-S. Ho, and H. Rabitz, *J. Chem. Phys.* **126**, 134303 (2007).
- [14] R. V. Mendes and V. I. Man'ko, *Phys. Rev. A* **67**, 053404 (2003).
- [15] P. Facchi, S. Tasaki, S. Pascazio, H. Nakazato, A. Tokuse, and D. A. Lidar, *Phys. Rev. A* **71**, 022302 (2005).
- [16] C. Altafini, *Phys. Rev. A* **70**, 062321 (2004).
- [17] C. Altafini, *J. Math. Phys.* **44**, 2357 (2003).
- [18] G. Lindblad, *Commun. Math. Phys.* **48**, 119 (1976).
- [19] V. Gorini, A. Kossakowski, and E. C. G. Sudarshan, *J. Math. Phys.* **17**, 821 (1976).
- [20] F. Shuang and H. Rabitz, *J. Chem. Phys.* **124**, 154105 (2006).
- [21] W. Zhu and H. Rabitz, *J. Chem. Phys.* **118**, 6751 (2003).
- [22] D. J. Tannor and A. Bartana, *J. Phys. Chem. A* **103**, 10359 (1999).
- [23] H. Jirari and W. Potz, *Phys. Rev. A* **72**, 013409 (2005).
- [24] M. Wenin and W. Potz, *Phys. Rev. A* **74**, 022319 (2006).
- [25] D. Sugny, C. Kontz, and H. Jauslin, *Phys. Rev. A* **74**, 053411 (2006).
- [26] D. Sugny, M. Ndong, D. Lauvergnat, Y. Justum, and M. Desouter-Lecomte, *J. Photochem. Photobiol. A : Chem* **in press** (2007).
- [27] V. Jurdjevic, *Geometric Control Theory* (Cambridge University Press, Cambridge, 1996).



- [28] U. Boscain and B. Picolli, *Optimal Syntheses for Control Systems on 2-D manifolds* (Springer SMAI, VOL. 43, 2004).
- [29] B. Bonnard and M. Chyba, *Singular trajectories and their role in control theory* (Springer SMAI, VOL. 40, 2003).
- [30] U. Boscain, G. Charlot, J.-P. Gauthier, S. Guérin, and H. R. Jauslin, *J. Math. Phys.* **43**, 2107 (2002).
- [31] U. Boscain and P. Mason, *J. Math. Phys.* **47**, 062101 (2006).
- [32] U. Boscain and Y. Chitour, *SIAM, J. Control Opt.* **44**, 111 (2005).
- [33] U. Boscain, T. Chambrion, and J.-P. Gauthier, *J. Dyn. Control Syst.* **8**, 547 (2002).
- [34] N. Khaneja, R. Brockett, and S. J. Glaser, *Phys. Rev. A* **63**, 032308 (2001).
- [35] N. Khaneja, S. J. Glaser, and R. Brockett, *Phys. Rev. A* **65**, 032301 (2002).
- [36] H. Yuan and N. Khaneja, *Phys. Rev. A* **72**, 040301 (2005).
- [37] D. Sugny, A. Keller, O. Atabek, D. Daems, C. M. Dion, S. Guérin, and H. R. Jauslin, *Phys. Rev. A* **71**, 063402 (2005).
- [38] D. Sugny, A. Keller, O. Atabek, D. Daems, C. M. Dion, S. Guérin, and H. R. Jauslin, *Phys. Rev. A* **72**, 032704 (2005).
- [39] D. Daems, S. Guérin, D. Sugny, and H. R. Jauslin, *Phys. Rev. Lett.* **94**, 153003 (2005).
- [40] D. Stefanatos, N. Khaneja, and S. J. Glaser, *Phys. Rev. A* **69**, 022319 (2004).
- [41] L. S. Pontryagin, *The Mathematical Theory of the Optimal Process* (Wiley-Interscience, New York, 1962).
- [42] S. Schirmer, *J. Phys. A* **37**, 1389 (2004).
- [43] H. Fu, S. G. Schirmer, and A. I. Solomon, *J. Phys. A* **34**, 1679 (2001).

# Time optimal control of a two-level dissipative quantum system

D. Sugny,\* C. Kontz, and H. R. Jauslin

*Institut Carnot, UMR CNRS 5027, BP 47870, 21078 Dijon, France*

(Dated: October 23, 2018)

We propose an analysis of the time-optimal control of a dissipative two-level quantum system whose dynamics is governed by the Lindblad equation. This simple system allows one to use tools of geometric control theory and to construct its optimal synthesis i.e. to determine the set of all the optimal trajectories starting from a given initial point. We study different processes such as conversion of a pure state into a mixed-state and purification of a mixed-state. In particular cases, we show that dissipation is not undesirable and can help accelerating the control.

PACS numbers: 32.80.Qk,03.65.Yz,78.20.Bh

## I. INTRODUCTION

Manipulating quantum system by using time-dependent electric field remains a goal of primary interests in different physical processes extending from the control of chemical reactions [?] to quantum computing [?]. In recent years, active research has been performed to take into account the interaction of the system with the environment which represents more realistic situations but also more challenging control scenarios than for closed quantum systems [?]. Different control strategies have been proposed. In this paper we will not consider control techniques using non-unitary control such as measurement (see for instance the quantum Zeno effect) [?], or other strategies such as bang-bang pulses, strong coupling with another system or control that can actively act on the dissipation (see [?] for a recent review and references therein). It has been shown that such methods are particularly efficient and can even halt decoherence. We restrict our study to unitary control. In this case and for the interaction with a markovian or a non-markovian bath, the fact that the control field cannot fully compensate the effect of dissipation largely enhances the difficulty of the control. This point has been rigorously shown in Refs. [?] for a dynamics governed by the Lindblad equation [?]. In this context, several studies using numerical optimization techniques have proved that efficient control can still be achieved [?]. Due to the complexity of realistic systems with multiple degrees of freedom, this purely numerical approach seems to be the only possible way to achieve control. More geometrical aspects of the control using mainly tools of geometric control theory [?] can be formulated only for simplest quantum systems having few levels (typically two or three) or consisting in the coupling of spin 1/2 particles. This has been done recently by a large number of mathematical papers dealing with closed [?] or dissipative [?] quantum systems. One of the objectives of the control has been the minimization of the

total time of the process either with constraints [?] or no constraints on the laser intensity [?].

In this paper, we propose to do a step towards the geometrical analysis of the control of dissipative quantum systems by beginning with the simplest system possible, a two-level system governed by the Lindblad equation. We determine control fields which minimize the total time of the process by applying the Pontryagin maximum principle (PMP) [?]. The maximum of the laser intensity is fixed to an arbitrary value. An increase of this value leads to a reduction of the duration of the control. Note also that this cost functional seems particularly relevant in the context of a dissipative environment especially when the effect of dissipation is undesirable to reach the objective of the control. A second argument explaining our choice of cost functional is of mathematical nature. The resolution of the PMP is particularly simple in this case and can be done analytically. The geometrical description of the time-optimal control is also well developed especially on  $\mathbb{R}^2$  (see [?] for a recent overview) for affine systems with a drift term corresponding here to the dissipation. The main tools of this construction will be recalled throughout the paper. Finally, all this mathematical arsenal allows us to answer some physical questions such as the benefit that can be gained from dissipation.

The paper is organized as follows. We first introduce the model for the Lindblad equation of a two-level system. Writing the density matrix in the coherence vector form [?] and assuming some constraints on the control term, we restrict the problem to a control on a closed submanifold of  $\mathbb{R}^2$  with a true drift term i.e. an uncontrollable term which cannot be eliminated by a unitary transformation. This drift term is due to the dissipation. We consider different cases with different initial and target states that represent several situations of physical interest. We formulate in Sec. III the PMP with a time minimum cost functional. In Sec. IV, we analyze the structure of the reachable set from each initial state and we point out the particular role of the fixed point of the free-dynamics in this structure. Section V deals with the construction of the optimal syntheses by solving the PMP. We recall that the PMP allows us to derive extremal controls. Optimal trajectories are a subset of this

---

\*Electronic address: dominique.sugny@u-bourgogne.fr

set which can be determined in a second step by a direct comparison of different extremal trajectories or by geometrical arguments. Conclusions and prospective views are given in Sec.VI. Some technical calculations are reported in appendices A and B.

## II. THE MODEL SYSTEM

We consider a dissipative two-level quantum system whose dynamics is governed by the Lindblad equation. The system is described by a density operator  $\rho(t)$  which is a positive semi-definite hermitian operator acting on a two-dimensional Hilbert space  $\mathcal{H}$ . The evolution equation can be written as

$$i\frac{\partial\rho}{\partial t} = [H_0 + uH_1, \rho] + i\mathcal{L}_D(\rho), \quad (1)$$

where  $H_0$  is the field-free Hamiltonian of the system,  $H_1$  represents the interaction with the control field and  $\mathcal{L}_D$  the dissipative part of the equation. In the Lindblad equation,  $\mathcal{L}_D$  can be written in the general form

$$\sum_{k=1}^3 [L_k \rho L_k^\dagger - \frac{1}{2}(\rho L_k^\dagger L_k + L_k^\dagger L_k \rho)], \quad (2)$$

where the operators  $L_k$  are given by

$$L_1 = \sqrt{\gamma_{21}} \begin{pmatrix} 0 & 1 \\ 0 & 0 \end{pmatrix}; L_2 = \sqrt{\gamma_{12}} \begin{pmatrix} 0 & 0 \\ 1 & 0 \end{pmatrix}; L_3 = \sqrt{\tilde{\Gamma}} \begin{pmatrix} 1 & 0 \\ 0 & -1 \end{pmatrix}$$

$\gamma_{12}$ ,  $\gamma_{21}$  and  $\tilde{\Gamma}$  are positive real constants describing the interaction with the environment.  $\gamma_{12}$  and  $\gamma_{21}$  correspond to population relaxations whereas  $\tilde{\Gamma}$  is the pure dephasing rate. We consider resonant fields, i.e. the frequency  $\omega$  of the laser is equal to the energy difference between the two levels. In the RWA approximation, the time evolution of  $\rho(t)$  satisfies the following Redfield form of the Lindblad equation

$$i\frac{\partial}{\partial t} \begin{pmatrix} \rho_{11} \\ \rho_{12} \\ \rho_{21} \\ \rho_{22} \end{pmatrix} = \begin{pmatrix} -i\gamma_{12} & -u^*e^{-i\omega t} & ue^{i\omega t} & i\gamma_{21} \\ -ue^{i\omega t} & -\omega - i\Gamma & 0 & ue^{i\omega t} \\ u^*e^{-i\omega t} & 0 & \omega - i\Gamma & -u^*e^{-i\omega t} \\ i\gamma_{12} & u^*e^{-i\omega t} & -ue^{i\omega t} & -i\gamma_{21} \end{pmatrix} \begin{pmatrix} \rho_{11} \\ \rho_{12} \\ \rho_{21} \\ \rho_{22} \end{pmatrix}$$

where  $u$  is the complex Rabi frequency of the laser field (the real and imaginary parts are the amplitudes of two orthogonal linearly polarized fields).  $\Gamma$  is the total dephasing rate which can be written as

$$\Gamma = \frac{1}{2}(\gamma_{12} + \gamma_{21}) + \tilde{\Gamma}. \quad (5)$$

From Eqs. (5), we also notice that the requirement that Eq. (4) corresponds to a Lindblad equation implies the constraint  $\Gamma \geq \frac{1}{2}(\gamma_{12} + \gamma_{21})$  or equivalently  $\tilde{\Gamma} \geq 0$ . Equation (4) is written in units such that  $\hbar = 1$ . In the interaction representation, Eq. (4) becomes

$$i\frac{\partial}{\partial t} \begin{pmatrix} \tilde{\rho}_{11} \\ \tilde{\rho}_{12} \\ \tilde{\rho}_{21} \\ \tilde{\rho}_{22} \end{pmatrix} = \begin{pmatrix} -i\gamma_{12} & -u^* & u & i\gamma_{21} \\ -u & -i\Gamma & 0 & u \\ u^* & 0 & -i\Gamma & -u^* \\ i\gamma_{12} & u^* & -u & -i\gamma_{21} \end{pmatrix} \begin{pmatrix} \tilde{\rho}_{11} \\ \tilde{\rho}_{12} \\ \tilde{\rho}_{21} \\ \tilde{\rho}_{22} \end{pmatrix}. \quad (6)$$

Since  $\text{Tr}[\rho] = 1$ , the density matrix  $\rho$  depends on three real parameters which can be given by the coordinates of the coherence vector [?] :  $x_1 = 2\Re[\tilde{\rho}_{12}]$ ,  $x_2 = 2\Im[\tilde{\rho}_{12}]$  and  $x_3 = \tilde{\rho}_{22} - \tilde{\rho}_{11}$ . From Eq. (6), one deduces that the coordinates  $x_i$  satisfy the following system of inhomogeneous linear differential equations

$$\begin{cases} \dot{x}_1 = -\Gamma x_1 + u_2 x_3 \\ \dot{x}_2 = -\Gamma x_2 - u_1 x_3 \\ \dot{x}_3 = (\gamma_{12} - \gamma_{21}) - (\gamma_{12} + \gamma_{21})x_3 + u_1 x_2 - u_2 x_1 \end{cases}, \quad (7)$$

$u_1$  and  $u_2$  being two real functions such that  $u = u_1 + iu_2$ . As  $\text{Tr}[\rho^2] \leq 1$ , we also have  $x_1^2 + x_2^2 + x_3^2 \leq 1$  which defines the Bloch ball. The dynamics is called either unital if  $\gamma_{12} = \gamma_{21}$  i.e. the fixed point of the free dynamics is the center of the Bloch ball or affine otherwise [? ?].

To simplify the study, we restrict the dynamics to a submanifold  $M \subset \mathbb{R}^2$  by assuming that the control field is real i.e.  $u_2 = 0$ . This hypothesis means that the control field is linearly polarized. With this choice of control, the last two equations of the system of Eqs. (7) are decoupled from the first one and the problem is reduced to  $\mathbb{R}^2$ . The system of Eqs. (7) then becomes

$$\begin{cases} \dot{x}_2 = -\Gamma x_2 - ux_3 \\ \dot{x}_3 = \gamma_- - \gamma_+ x_3 + ux_2 \end{cases}, \quad (8)$$

where  $\gamma_- = \gamma_{12} - \gamma_{21}$  and  $\gamma_+ = \gamma_{12} + \gamma_{21}$ . The coordinate  $x_1$  is set initially to 0. To simplify the notation, the index of  $u_1$  has been omitted when confusion is unlikely to occur. Note that the analysis of the optimal control on  $\mathbb{R}^3$  is considerably more complex [?] and goes beyond the scope of this paper. Equations (8) can be written in a more compact form

$$\dot{\mathbf{x}} = F + uG, \quad (9)$$

with the vector  $\mathbf{x}$  of coordinates  $(x_2, x_3)$  and the two vector fields  $F$  and  $G$  defined by

$$F = \begin{pmatrix} -\Gamma x_2 \\ \gamma_- - \gamma_+ x_3 \end{pmatrix} \text{ and } G = \begin{pmatrix} -x_3 \\ x_2 \end{pmatrix}. \quad (10)$$

Finally, a straightforward calculation shows that the fixed point of the free-dynamics is given for  $\gamma_+ \neq 0$  by

$$\begin{cases} x_2 = 0 \\ x_3 = \frac{\gamma_-}{\gamma_+} \end{cases}, \quad (11)$$

which is therefore either affine or unital according to the value of  $\gamma_-$ . The irreversibility of the dissipation effects is reflected in the fact that the vector field  $F$  is a true drift term which cannot be eliminated by unitary transformations [?].

## III. PONTRYAGIN MAXIMUM PRINCIPLE

We analyze the optimal control of this two-level system with the constraint of minimizing the total time of the control. We assume that the field  $u$  is bounded by

$$|u| \leq 1. \quad (12)$$

Equations (8) being linear, other bounds for  $u$  can be considered from a standard rescaling of the time and the dissipative constants  $\Gamma$ ,  $\gamma_+$  and  $\gamma_-$ . The Pontryagin maximum principle [? ? ? ?] is formulated from the following pseudo-Hamiltonian  $H_P$

$$H_P = \mathbf{p} \cdot (F + uG) + p_0, \quad (13)$$

where  $\mathbf{p} = (p_2, p_3) \in (\mathbb{R}^2)^*$  is called the adjoint state and  $p_0$  is a negative constant. We recall that the cost function for the minimum time problem is equal to 1. This term is multiplied by the constant  $p_0$  in the Hamiltonian  $H_P$ . The Pontryagin maximum principle states that the extremal trajectories maximize  $H_P$  i.e.

$$H_{max}(\mathbf{x}, \mathbf{p}) = \text{Max}_{|u| \leq 1} H_P(\mathbf{x}, \mathbf{p}, u). \quad (14)$$

The coordinates of the extremal vector state  $\mathbf{x}$  and of the corresponding adjoint state  $\mathbf{p}$  fulfill the Hamilton equations

$$\begin{cases} \dot{x}_2 = -\Gamma x_2 - u x_3 \\ \dot{x}_3 = \gamma_- - \gamma_+ x_3 + u x_2 \end{cases}, \quad (15)$$

and

$$\begin{cases} \dot{p}_2 = \Gamma p_2 - u p_3 \\ \dot{p}_3 = \gamma_+ p_3 + u p_2 \end{cases}, \quad (16)$$

where  $u$  is here the extremal control given by Eq. (14).

We can now pass to the construction of the optimal syntheses. The construction begins with the introduction of two sets of points  $\Delta_A^{-1}(0)$  and  $\Delta_B^{-1}(0)$  denoted  $C_A$  and  $C_B$  which divide  $M$  in different regions [?].  $\Delta_A$  and  $\Delta_B$  are two functions from  $M$  to  $\mathbb{R}$  defined as follows

$$\begin{cases} \Delta_A(\mathbf{x}) = \text{Det}(F, G) \\ \Delta_B(\mathbf{x}) = \text{Det}(G, [F, G]) \end{cases}, \quad (17)$$

where  $\text{Det}$  is the determinant of two vector fields and  $[.,.]$  their commutator. In our case, simple algebra leads to

$$\begin{cases} \Delta_A(\mathbf{x}) = -\Gamma x_2^2 + \gamma_- x_3 - \gamma_+ x_3^2 \\ \Delta_B(\mathbf{x}) = 2\Gamma x_2 x_3 - 2\gamma_+ x_2 x_3 + \gamma_- x_2 \end{cases}. \quad (18)$$

The major role of these two sets in the resolution of the optimal control problem will be detailed in Sec. V. We can already say that  $C_A$  and  $C_B$  are responsible for qualitative modifications of the optimal trajectories [? ?]. A preliminary step thus consists in analyzing the structure of the sets  $C_A$  and  $C_B$  when  $\Gamma$ ,  $\gamma_+$  and  $\gamma_-$  vary with the conditions  $\gamma_+ \geq 0$  and  $\Gamma \geq \frac{\gamma_+}{2}$ . From a formal point of view, this can be done by introducing the feed-back group [?] but the dynamics being here bilinear [Eqs. (8)], we can directly compute the sets  $C_A$  and  $C_B$  and their relative positions.

If  $\Gamma \neq \gamma_+$  then the set  $C_B$  corresponds to the union of the two lines

$$x_2 = 0, \quad (19)$$

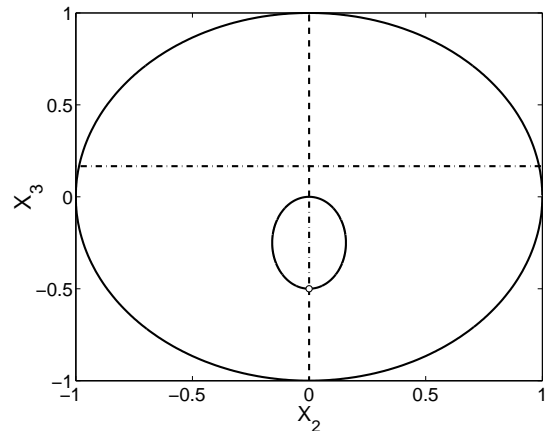


FIG. 1: Division of the manifold  $M$  by the sets  $C_A = \Delta_A^{-1}(0)$  (in solid line) and  $C_B = \Delta_B^{-1}(0)$  (in dashed and dot-dashed lines) for  $\gamma_- \neq 0$ . The dashed and dot-dashed lines represent respectively anti-turnpike and turnpike arcs which are introduced in Sec. V. The exterior circle in solid line corresponds to the limit of the Bloch ball in the plane  $(x_2, x_3)$ . The small open circle indicates the position of the fixed-point of the free dynamics. Numerical values are taken to be  $\Gamma = 1$ ,  $\gamma_{12} = 0.1$  and  $\gamma_{21} = 0.3$ .

and

$$x_3 = \frac{-\gamma_-}{2\Gamma - 2\gamma_+}, \quad (20)$$

with the restriction that  $|x_3| \leq 1$ . In the case  $\Gamma = \gamma_+$ ,  $C_B$  is only composed of the vertical line of equation  $x_2 = 0$ . The points  $(x_2, x_3)$  of the Bloch ball that are solutions of the polynomial equation  $\gamma_+ x_3^2 - \gamma_- x_3 - \Gamma x_2^2 = 0$  belong to  $C_A$ . In the case  $\gamma_- \neq 0$ ,  $C_A$  is therefore the union of two parabolas. This set is either above or below the line  $x_3 = \frac{-\gamma_-}{2\Gamma - 2\gamma_+}$  according to the signs of  $\gamma_-$  and of  $\Gamma - \gamma_+$ . For  $\gamma_- = 0$ , this set is reduced to the origin of the Bloch ball. Figure 1 displays the submanifold  $M$  together with the sets  $C_A$  and  $C_B$  for a given value of the parameters. We finally notice that the fixed-point of the free dynamics and the center of the Bloch ball belong to  $C_A$ .

#### IV. REACHABLE SETS AND CONTROLLABILITY

We consider four different qualitative cases of control which allow one to study several physically relevant situations :

- Case (a) : Conversion of a pure state into a mixed state with a unital Lindbladian ( $\gamma_-/\gamma_+ = 0$ ,  $\Gamma > \gamma_+ + 2$ ).
- Case (b) : Conversion of a pure state into a mixed state with a unital Lindbladian ( $\gamma_-/\gamma_+ = 0$ ,  $\gamma_+ - 2 < \Gamma < \gamma_+ + 2$ ).

- Case (c) : Purification of the completely random mixed state which corresponds to the center of the Bloch ball ( $\gamma_-/\gamma_+ = -1, \Gamma > \gamma_+ + 2$ ).
- Case (d) : Conversion of a pure state into a mixed state with an affine Lindbladian ( $\gamma_-/\gamma_+ = -0.5, \Gamma > \gamma_+ + 2$ ).

The numerical values we have chosen for illustrations are given in Table I. Although the choice of the parameters

TABLE I: Numerical values of the dissipative constants in arbitrary units.

	$\Gamma$	$\gamma_{12}$	$\gamma_{21}$
(a)	3	0.3	0.3
(b)	1.5	0.3	0.3
(c)	3	0	1
(d)	3	0.1	0.3

of Table I will become clearer in Sec. V, some comments can already be made. This choice both depends on the structure of the sets  $C_A$  and  $C_B$  and on the characteristics of two particular extremals denoted  $X^-$  and  $Y^-$  which start at the initial point, and correspond respectively to a constant control equal to -1 and 1. As detailed in the appendix B, the  $X^-$  and  $Y^-$  trajectories are either pseudo-periodic or aperiodic according to the sign of the discriminant  $\Delta = (\Gamma - \gamma_+)^2 - 4$  of the system of Eqs. (8). An exact resolution of the dynamics shows that the trajectory of the system is aperiodic if  $\Delta > 0$  and pseudo-periodic otherwise. This point is summarized by the diagram 10 of the appendix B. In Table I, we have chosen for three of the four examples  $\Gamma$  such that  $\Gamma > \gamma_+ + 2$  to simplify the local structure of the optimal synthesis around the fixed-point of the dynamics. A pseudo-periodic trajectory is locally a spiral in the plane  $(x_2, x_3)$  around this fixed point which makes the analysis more complex (see Sec. V).

### A. Purity and limits of the dynamics

Before analyzing the reachable set and the controllability of each example, we begin by some general comments about the dynamics.

We first show that the field cannot locally compensate the effect of dissipation. The purity of the quantum state is defined by the function  $2\text{Tr}[\rho^2] - 1 = x_2^2 + x_3^2$ . Pure states are thus on the unit circle of the  $(x_2, x_3)$  plane. Simple algebra then leads to

$$\frac{d(\text{Tr}[\rho^2])}{dt} = -\Gamma x_2^2 + \gamma_- x_3 - \gamma_+ x_3^2, \quad (21)$$

and we notice that this derivative does not depend on  $u$ , which completes the proof. A more general proof of this point is given in Refs. [? ?]. We also point out that for

points  $\mathbf{x}$  where  $\Delta_A(\mathbf{x}) < 0$  then  $\frac{d\text{Tr}[\rho^2]}{dt} < 0$  and inversely if  $\Delta_A(\mathbf{x}) > 0$  then  $\frac{d\text{Tr}[\rho^2]}{dt} > 0$ . The curve  $C_A$  divides the plane  $(x_2, x_3)$  into a region where the purity of the state locally increases and a region where it locally decreases. On the boundary  $C_A$ , the purity is preserved. This point can be qualitatively understood as follows. We recall that the purity is equal to the square of the distance to the origin. The conservative vector field  $G$  is orthoradial (i.e. normal to radial vectors) for each point  $(x_2, x_3) \neq (0, 0)$  of the manifold. The dissipative vector field  $F$  does not modify the purity of the state if the radial component of  $F$  vanishes i.e. if  $F$  is parallel to  $G$  which is the definition of the curve  $C_A$ .

We next analyze the fixed points of the dynamics when the field is on, which are defined by  $F + uG = 0$ . Since  $F$  and  $G$  are parallel, the fixed points belong to the curve  $C_A$ . The field-free limit point is the point of this line of maximum purity (see for instance Fig. 1). This shows that the dissipation alone allows to reach the state of maximum purity. Inversely, one can ask if every point of the curve  $C_A$  corresponds to a limit point of the dynamics. The answer is positive for a real non-bounded control  $u$  since the limits can be written

$$\begin{cases} x_2 = \frac{-u\gamma_-}{\Gamma\gamma_+ + u^2} \\ x_3 = \frac{\gamma_-}{\gamma_+ + u^2/\Gamma} \end{cases}. \quad (22)$$

### B. Reachable sets

We begin by recalling some results of Refs. [? ?] about controllability of dissipative systems. A quantum dissipative system of finite dimension whose dynamics is governed by the Lindblad equation is generically accessible but not controllable. The accessibility property characterizes the fact that the system can be driven in every direction of the state space. Moreover, the concept of accessibility does not take into account the reversibility or the irreversibility of the process. The lack of controllability is measured by the non small-time controllability of the system which illustrates the irreversibility of the dynamics. This kind of system is not small-time controllable because the field cannot locally compensate the effect of dissipation as shown by Eq. (21). The accessibility property can be checked by the computation of the dimension of the dynamical Lie algebra  $L$  of the system [? ?]. We introduce for that purpose the density matrix  $\bar{\rho}$  of coordinates  $(1, x_2, x_3)$  which is given in the basis of the coherence vector and we rewrite Eqs. (8) in matrix form as follows

$$\dot{\bar{\rho}} = \mathcal{L}_F \bar{\rho} + u \mathcal{L}_G \bar{\rho}, \quad (23)$$

where  $\mathcal{L}_F$  and  $\mathcal{L}_G$  are  $3 \times 3$  matrices given by

$$\mathcal{L}_F = \begin{pmatrix} 0 & 0 & 0 \\ 0 & -\Gamma & 0 \\ \gamma_- & 0 & -\gamma_+ \end{pmatrix} \text{ and } \mathcal{L}_G = \begin{pmatrix} 0 & 0 & 0 \\ 0 & 0 & -1 \\ 0 & 1 & 0 \end{pmatrix}. \quad (24)$$

$L$  is the Lie algebra generated by  $\mathcal{L}_F$  and  $\mathcal{L}_G$ . If  $\Gamma \neq \gamma_+$ , a direct computation shows that  $L$  is either isomorphic to  $\mathfrak{gl}(2)$  or to the semi-direct sum  $\mathfrak{gl}(2) \ltimes \mathbb{R}^2$  of respective dimensions 4 and 6 for  $\gamma_- = 0$  or  $\gamma_- \neq 0$ . The system is therefore accessible for  $\Gamma \neq \gamma_+$ .

We now determine the reachable sets from their respective initial states of the four examples. The reachable sets can be constructed by the explicit construction of all the trajectories. We denote by  $\mathcal{R}(\mathbf{x}_0)$  the reachable set from  $\mathbf{x}_0$ . We first search for in this section the boundary of the reachable sets. Then in Sec. V we show that all the points inside the boundary are attainable. We consider for that the  $X-$  and  $Y-$  trajectories starting from the initial point and from the field-free fixed point of the dynamics. A qualitative change occurs when the  $X-$  or  $Y-$  trajectories cross  $C_A$  since the angle between the vector  $F(\mathbf{x})$  and  $G(\mathbf{x})$  changes its sign. The determination of all the extremal trajectories in Sec. V allows us to complete the construction.

We apply these remarks to the cases (a) and (b) where the initial point has coordinates  $(x_2 = 0, x_3 = 1)$  and  $C_A$  is reduced to the origin  $(x_2 = 0, x_3 = 0)$ . The origin is attained asymptotically by the dynamics when  $t \rightarrow +\infty$ . The  $Y-$  and  $X-$  trajectories, which have the same initial and final points, are therefore global boundaries of the reachable set. This point is illustrated in Figs. 2a and 2b for the cases (a) and (b), where the reachable set  $\mathcal{R}$  is in grey.

For the case (c), the  $X-$  and  $Y-$  trajectories starting from  $(x_2 = 0, x_3 = 0)$  intersect asymptotically  $C_A$ . We also consider the  $X-$  and  $Y-$  trajectories starting from the field-free fixed point which define two new regions. As an infinite time is necessary to reach this point, these two trajectories do not belong to the reachable set.  $\mathcal{R}$  is the union of all these regions as shown in Fig. 2c. We will check in Sec. V by constructing the extremal trajectories that every point of this set is effectively attainable.

For the case (d) the situation is more difficult to analyze as the  $X-$  and  $Y-$  trajectories starting from  $(x_2 = 0, x_3 = 1)$  intersect transversally  $C_A$ . From this point of intersection, the two trajectories do not correspond anymore to the boundary of  $\mathcal{R}$ . After the crossing of  $C_A$ , the  $X-$  or  $Y-$  trajectories originating from the preceding curves define two new regions of  $\mathcal{R}$ . We finally consider the limit point of the field-free dynamics which can be attained as  $t \rightarrow +\infty$  and the  $X-$  and  $Y-$  trajectories starting from this point. These two lines define two new boundaries which intersect asymptotically  $C_A$  but which do not belong to  $\mathcal{R}$ .  $\mathcal{R}$  is therefore composed of all the regions constructed above and is displayed in Fig. 2d. As before, only the determination of the extremal trajectories will complete the construction.

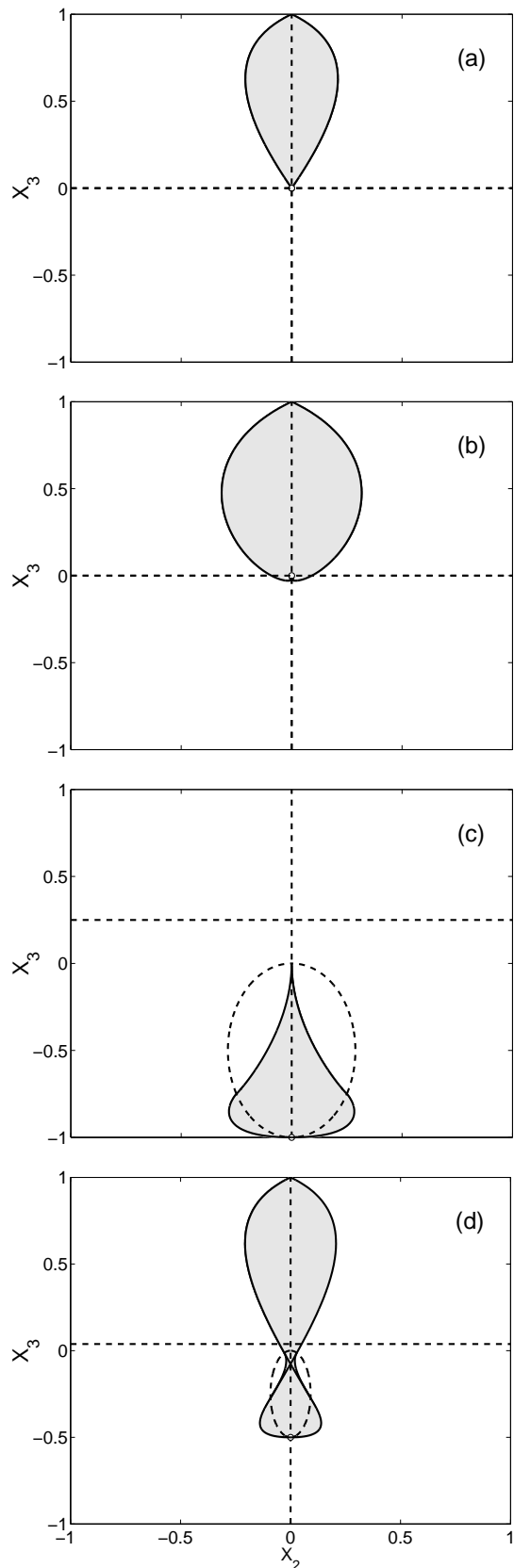


FIG. 2: Reachable sets  $\mathcal{R}$  (in grey) for the cases (a), (b), (c) and (d). The sets  $C_A$  and  $C_B$  are represented in dashed lines. The position of the field-free fixed point is indicated by the small open circle. In (c) and (d), the trajectories starting from the field-free fixed point do not belong to  $\mathcal{R}$  (see text).

## V. TIME-OPTIMAL CONTROL

The application of the Pontryagin maximum principle is particularly simple at least locally in the case of time minimum control. The goal of this section is to solve this problem by constructing the optimal synthesis i.e. the set of all the optimal solutions starting from a given initial point  $\mathbf{x}_0$  and reaching a point of  $\mathcal{R}(\mathbf{x}_0)$ . For time optimization, the optimal controls are composed of piecewise constant parts ( $u = \pm 1$ ) and of singular controls. Some preliminary work in Sec. V A has to be done before determining the optimal solutions.

### A. Preliminary

We define two functions  $\Phi$  and  $\theta$  [? ].  $\Phi$ , called the switching function, is given by

$$\Phi(t) = \mathbf{p} \cdot \mathbf{G} = -p_2 x_3 + p_3 x_2. \quad (25)$$

Using Eq. (13), standard considerations of maximization of the pseudo-Hamiltonian  $H_P$  lead to the conclusion that the extremal field at time  $t$  is given by  $u = \text{sign}(\Phi(t))$  if  $\Phi(t) \neq 0$ . A time  $t_0$  such that the control changes sign (i.e. such that  $\Phi(t_0) = 0$ ) is a switching time. If  $\Phi$  vanishes on an interval  $[t_0, t_1]$  then the corresponding trajectory is called singular and is referred to as a  $Z$ -trajectory. An important point is the fact that the  $Z$ -trajectories lie in the set  $C_B$  and that the corresponding control  $u = \phi$  is singular i.e. different from 1 or -1.  $\phi$  can be calculated by imposing that  $\frac{d}{dt} \Delta_B(\mathbf{x}(t)) = 0$  on  $[t_0, t_1]$ . In our case, it can be shown that

$$\frac{d}{dt} \Delta_B(\mathbf{x}(t)) = 0 = \frac{\partial \Delta_B}{\partial x_2} \dot{x}_2 + \frac{\partial \Delta_B}{\partial x_3} \dot{x}_3. \quad (26)$$

One arrives after simple algebra to

$$\phi(\mathbf{x}) = \frac{-x_2 \gamma_- (\Gamma - 2\gamma_+) - 2x_2 x_3 (\gamma_+^2 - \Gamma^2)}{2(\Gamma - \gamma_+) (x_2^2 - x_3^2) - \gamma_- x_3}. \quad (27)$$

For the line  $x_2 = 0$  of  $C_B$ , this leads to  $\phi(\mathbf{x}) = 0$ . For the line  $x_3 = \frac{-\gamma_-}{2(\Gamma - \gamma_+)}$ , we obtain

$$\phi(\mathbf{x}) = \frac{\gamma_- (\gamma_+ - 2\Gamma)}{2(\Gamma - \gamma_+) x_2}. \quad (28)$$

The control is admissible if  $|\phi(\mathbf{x})| \leq 1$  which implies here the condition

$$|x_2| \geq \left| \frac{\gamma_- (\gamma_+ - 2\Gamma)}{2(\Gamma - \gamma_+)} \right|. \quad (29)$$

Not every  $Z$ -trajectory can be an optimal trajectory. We introduce to characterize this point the notion of turnpike and anti-turnpike curves [? ]. Let  $\mathbf{x} \notin C_A \cup C_B$  and the function  $f(\mathbf{x}) = -\frac{\Delta_B(\mathbf{x})}{\Delta_A(\mathbf{x})}$ . A turnpike curve is an arc lying in  $C_B$  such that for every point  $\mathbf{x}$  of this arc

$\Delta_A(\mathbf{x}) \neq 0$  and  $X(\mathbf{x})$  and  $Y(\mathbf{x})$  are not tangent to  $C_B$ . It is also assumed that  $X(\mathbf{x})$  and  $Y(\mathbf{x})$  point to opposite sides of  $C_B$  which define two regions  $\Omega_x$  and  $\Omega_y$ . If  $f(\mathbf{x}) > 0$  (resp.  $f(\mathbf{x}) < 0$ ) on  $\Omega_y$  and  $f(\mathbf{x}) < 0$  (resp.  $f(\mathbf{x}) > 0$ ) on  $\Omega_x$  then the arc is a turnpike (resp. anti-turnpike) arc. The relation with the optimal synthesis can be stated as follows. Using for instance the clock form  $\alpha$  (see appendix A), it can be shown that the anti-turnpike trajectories are not optimal. Figure 1 displays the turnpike and the anti-turnpike curves for particular values of the parameters.

The switching function  $\Phi$  is a powerful tool that gives all the informations on the extremal trajectory. However, a global analysis of the extremals using only  $\Phi$  is difficult because all the initial values  $(p_{20}, p_{30})$  have to be tested. A more global point of view is given by the function  $\theta$  which has the advantage not to depend on  $\mathbf{p}$ .

Let  $\mathbf{v}$  be the vector of coordinates  $(\dot{x}_2, \dot{x}_3)$ . Deriving Eqs. (8) with respect to time, it can be shown that  $\mathbf{v}$  satisfies the following system of equations

$$\begin{cases} \dot{v}_2 = -\Gamma v_2 - u v_3 \\ \dot{v}_3 = -\gamma_+ v_3 + u v_2 \end{cases}. \quad (30)$$

We next introduce the vector  $\tilde{v}(t)$ . At time  $t$ , let us assume that the dynamics reaches the point  $(x_2(t), x_3(t))$  and that the vector field  $G$  at this point is given by  $G(x_2(t), x_3(t)) = G(t)$ .  $\tilde{v}(t)$  is defined as the solution at time 0 of Eqs. (30) that at time  $t$  is equal to  $G(t)$ . The dynamics is thus propagated backwards during the time  $t$ .  $\theta$  is then defined as

$$\theta(t) = \arg(\tilde{v}(0), \tilde{v}(t)), \quad (31)$$

where the angle is measured counterclockwise. The definition of  $\theta$  originates from the fact that the product  $\mathbf{p}(t) \cdot \mathbf{v}(t)$  is a constant [? ]. We thus have

$$\Phi(t) = p(t) \cdot G(t) = p(0) \cdot \tilde{v}(t). \quad (32)$$

The function  $\theta$  allows to determine some properties of the extremal trajectories. We briefly recall these points here. The reader is referred to [? ] for rigorous definitions and complete proofs. It can first be shown that

$$\text{sign}(\dot{\theta}) = \text{sign}(\Delta_B), \quad (33)$$

which means that the zeros of  $\dot{\theta}$  are located on  $C_B$ . A switch can occur if  $\dot{\theta} > 0$  and  $\theta > 0$  or  $\dot{\theta} < 0$  and  $\theta < 0$ . In addition, the variation of  $\theta$  between two switches or between a switch and a singular control is equal to 0 modulo  $\pi$ . This latter point can be easily understood from Eq. (32). Other properties of  $\theta$  will be detailed during the construction of the optimal synthesis.

### B. Time-optimal syntheses

The parts V B 1, V B 2, V B 3 and V B 4 are rather technical and describe the way to obtain the optimal syntheses. Section V B 5 details conclusions on the role of the

dissipation that can be gained from the resolution of the time optimal control.

### 1. Case (a)

In the case (a), the optimal trajectories are either bang or bang-bang. A bang trajectory is a trajectory associated to a single value of the control  $u = +1$  or  $u = -1$ . A bang-bang trajectory is the concatenation of an  $X$ - and an  $Y$ - trajectories. We denote by  $X*Y$  such a concatenation where the  $Y$ - trajectory comes first. Here the maximum number of switches is thus equal to 1. The elimination of extremal trajectories selected by the Pontryagin maximum principle has been done through the clock form  $\alpha$  (see appendix A for details) and the symmetry of the diagram with respect to the line  $x_2 = 0$ . We recall that the clock form can only be used for trajectories belonging to one of the four quadrants defined by  $C_B$  and which do not cross  $C_A$ . Figure 3 displays the optimal synthesis for this problem and the evolution of the angle  $\theta$  along the  $Y$ - trajectory starting from the initial point  $(0, 1)$ . The plot of  $\theta$  shows that the switches are always permitted along the  $X$ - or the  $Y$ - trajectory. Note also that the form of the curve representing  $\theta$  is related to the sign of  $\Delta$ . More precisely, if  $\Gamma > \gamma_+ + 2$  then  $\theta$  is a monotonically decreasing function and if  $\Gamma < \gamma_+ - 2$  (case not treated here),  $\theta$  starts increasing, passes through a maximum when the trajectory crosses  $C_B$  and then decreases. The intermediate case  $\gamma_+ - 2 < \Gamma < \gamma_+ + 2$  corresponds to the case (b). Using the clock form, it can be shown that only one switch is possible for a trajectory in a given quadrant. This point can also be determined from more general considerations detailed in Ref. [?]. The rest of the optimal synthesis is deduced from the symmetry of the problem. The line  $x_2 = 0$  is called an overlap curve denoted by  $K$  as it is the locus of points reached by two optimal trajectories. We finally notice that the dissipation alone is not used here by the control and therefore cannot help accelerating the control. We recall that the singular control on the vertical line of  $C_B$  is given by  $u = 0$ .

### 2. Case (b)

The situation is a little more complex in the case (b). For  $x_3 > 0$ , the synthesis is similar to the one of case (a) i.e. the trajectories are either bang or bang-bang. The function  $\theta$  is here periodic, the times where  $\dot{\theta}$  vanishes correspond to the crossing of  $C_B$ . This function tells also us that the initial  $Y$ - and  $X$ - trajectories cannot switch in their respective second quadrant (i.e. the second quadrant they go through) since  $\dot{\theta}(t) > 0$  and  $\theta(t) < 0$ . By symmetry with respect to the line  $x_2 = 0$ , one deduces that these curves are optimal up to this line. A singular control along the horizontal line of  $C_B$  is optimal from the point of intersection between the initial  $X$ - or  $Y$ -

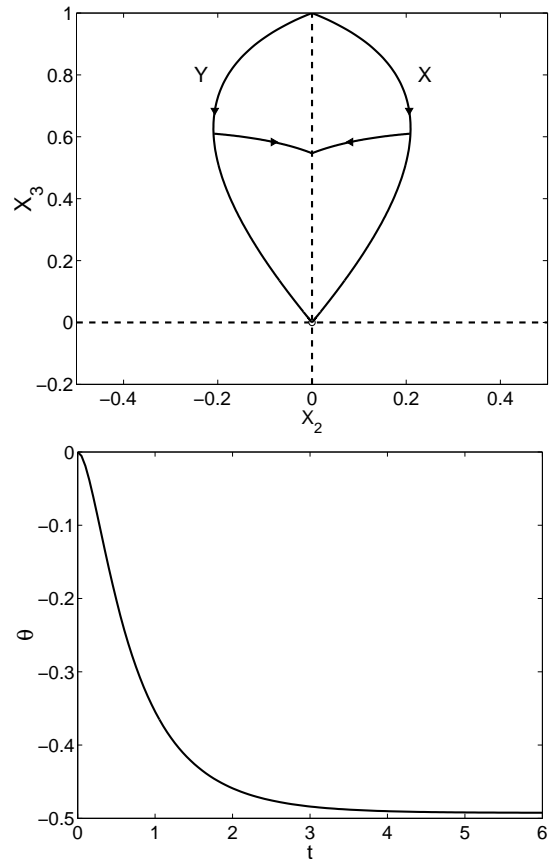


FIG. 3: The top figure represents the optimal synthesis for the case (a) (see text). The dashed lines indicate the locus  $C_B$  and the small open circle the fixed point of the dynamics. The bottom figure displays the evolution of  $\theta$  as a function of the time for the  $Y$ - trajectory starting from the point  $(0, 1)$ .

trajectories and this line. Since  $\gamma_- = 0$ , the singular control is given by  $\phi = 0$ . From this singular line originate optimal trajectories with control  $u = \pm 1$ . Using the clock form  $\alpha$ , it can be shown that these trajectories can not switch again. To summarize, in this second part we have constructed optimal controls of the form  $Y*Z*X$ ,  $Y*Z*Y$ ,  $X*Z*X$  and  $X*Z*Y$ . This optimal synthesis is represented in Fig. 4. Here, one sees that the dissipation alone (with  $u = 0$ ) accelerates the control to reach a point near the origin only along the horizontal direction and for  $x_3 = 0$ . We finally give in Fig. 5 an example of the comparison of two extremal trajectories. The time to reach respectively the points A and B from the initial point  $(0,1)$  by the  $Y$ - and  $X$ - trajectories is the same. We would like to attain the point C from A or B. We use either the  $X$ -trajectory from B or a concatenation of a  $Y$ - and a  $Z$ - ones from A. The clock form  $\alpha$  cannot be used here since the trajectories belong to two different quadrants. We therefore consider the symmetric image AD of the curve BD with respect to  $x_2 = 0$ . The two extremals are thus in the same quadrant and  $\alpha$  can be used. We conclude that the curve  $Y*Z*Y$  is optimal



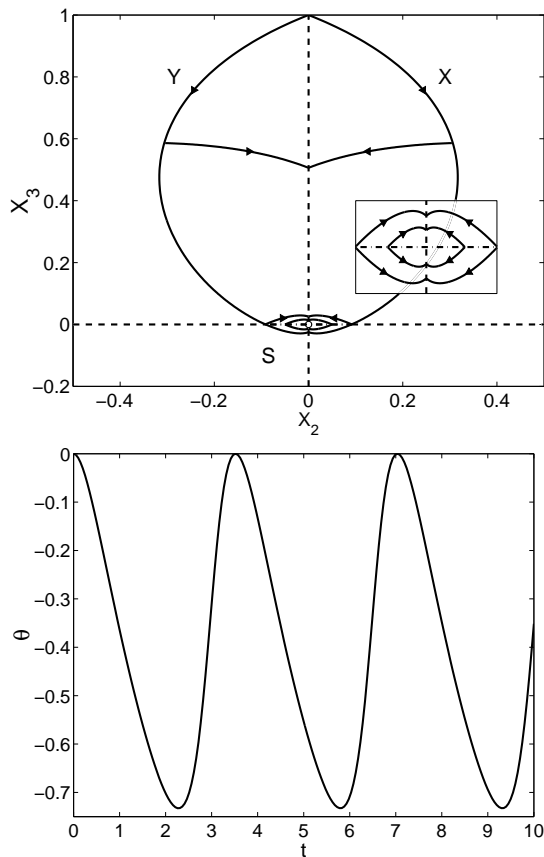


FIG. 4: Same as Fig. 3 but for the case (b). The dotted-dashed line represents the singular trajectory  $S$ . The small insert is a zoom of the optimal synthesis near the origin.

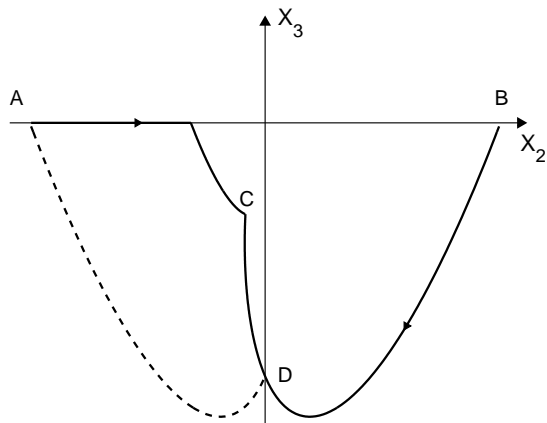


FIG. 5: Use of symmetry to determine the optimal trajectory (see text).

to reach the point  $C$ .

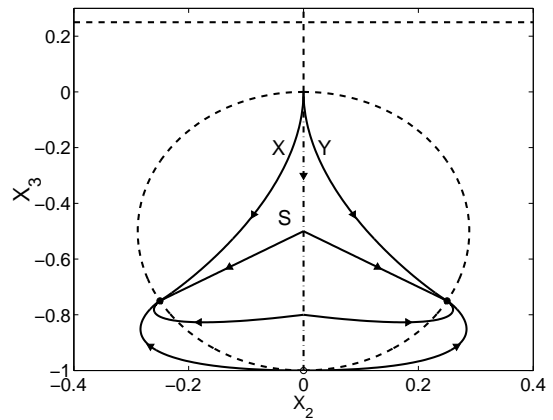


FIG. 6: Same as Fig. 4 but for the case (c).

### 3. Case (c)

In this case, the singular line  $x_2 = 0$  is optimal. The singular control is equal to zero. Switches can occur from the initial  $X-$  and  $Y-$  trajectories but they do not lead to optimal trajectories. Inversely,  $X-$  and  $Y-$  trajectories originating from  $S$  are found to be optimal. When two extremals cross  $C_A$ ,  $\alpha$  cannot be used and a direct numerical comparison is then performed. In this case, the function  $\theta$  tells us that these curves do not switch. Trajectories originating from  $S$  that have a switch are therefore not extremal. We finally point out that the dissipation is beneficial for the control and decreases the duration needed to purify the system. The optimal controls are here of the form  $X-, Y-, X*Z$  or  $Y*Z$ . Figure 6 displays the optimal synthesis for this problem.

### 4. Case (d)

The case (d) is the more complex one and corresponds roughly to the composition of cases (b) and (c). The difficulty lies in the global structure of the control or, in other words, in gluing the two preceding local analysis. For  $x_3 > 0$ , the optimal synthesis is similar to the cases (a) or (b) with bang or bang-bang trajectories. The bottom of the optimal synthesis from the point of intersection of the initial  $X-$  and  $Y-$  trajectories is similar to the case (c).

We now describe the central part of the synthesis. The horizontal singular line of  $C_B$  does not correspond to a singular trajectory since  $|\phi(\mathbf{x})| > 1$  which is a non-admissible control. Consider the first point of intersection of  $C_B$  with the  $X-$  or  $Y-$  trajectory. Following [?], we know that a switch curve  $C$  originates from this point. To determine the exact locus of  $C$ , we use the  $\theta$  function since this function varies by  $0$  modulo  $\pi$  between two switches.  $C$  is constructed numerically. By definition of  $C$ , every trajectory which crosses  $C$  switches on  $C$ . We have found that  $C$ ,  $C_B$  and  $C_A$  intersect in one

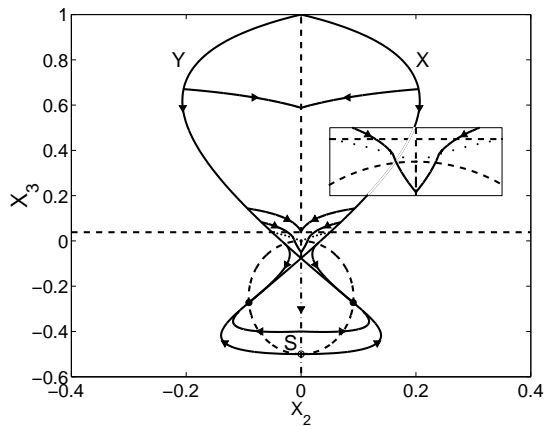


FIG. 7: Same as Fig. 4 but for the case (d). The dotted line represents the switch curve  $C$ .

point, the origin  $O$ .

Since the line  $x_2 = 0$  is turnpike for  $\frac{\gamma_-}{\gamma_+} < x_3 < 0$ , we can ask if this singular trajectory is optimal i.e. if we can have a local optimal synthesis of the form given by Fig. 8. To answer this question, we use the switching function  $\Phi$ . For  $\mathbf{x}(t) \in C \cup S$ ,  $\Phi(t) = 0$  i.e. the vectors  $\mathbf{p}(t)$  and  $G(\mathbf{x}(t))$  are orthogonal. Since the direction of  $G$  is known ( $G$  is orthoradial), one can deduce the direction of  $\mathbf{p}(t)$ . Let  $\mathbf{z}_1$  and  $\mathbf{z}_2$  be two points belonging respectively to  $C$  and  $S$ . The vectors  $G(\mathbf{z})$  associated to these points are schematically represented in Fig. 8. We let now the states  $\mathbf{z}_1$  and  $\mathbf{z}_2$  go to  $(0, 0)$  and we determine the directions of the different adjoint states. We recall that the Pontryagin maximum principle states that  $\mathbf{p}$  is a continuous function which does not vanish. When  $\mathbf{z}_1$  goes to  $(0, 0)$ , one deduces by a continuity argument that  $\mathbf{p}_1$  is vertical in  $O$ . When  $\mathbf{z}_2$  goes to  $(0, 0)$ , the limit direction of  $\mathbf{p}_2$  is given by the switch curve  $C$ . To respect the continuity of  $\mathbf{p}$ , one sees that  $C$  has to be tangent to the line  $x_2 = 0$  in  $O$ . Due to the complexity of analytical calculations, we have checked numerically that this is not the case. The singular line for  $x_3 < 0$  is therefore not optimal. The trajectories of the form  $Y * X * Y$  or  $X * Y * X$  are thus optimal up to  $x_2 = 0$ . In addition, when the initial  $X$ - and  $Y$ -trajectories cross  $C_A$ , the angle between the vectors  $F(\mathbf{x})$  and  $G(\mathbf{x})$  changes its sign. New optimal trajectories originate from this point of intersection and correspond to two new regions of the reachable set.

### 5. Qualitative conclusions on the dynamics

From the results obtained in the preceding sections, some qualitative conclusions can be made with respect to the dissipation effect on the time optimal control of the dynamics. The dissipation is not undesirable when the dissipation allows to purify the system [cases (c) and (d)] and help accelerating the control. In contrast for the conversion of a pure state into a mixed state, the dissi-

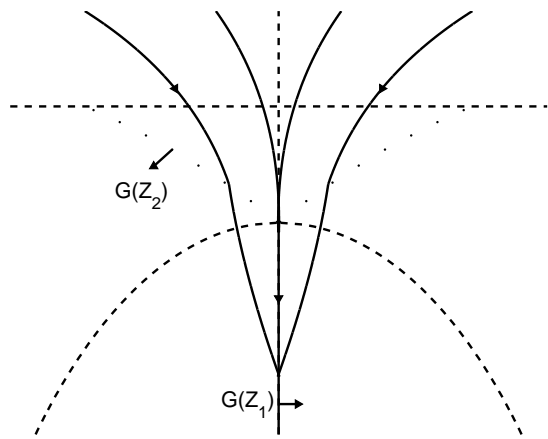


FIG. 8: Possible optimal synthesis around the origin.

pation alone increases the duration of the control and its effect is not beneficial for the control [cases (a) and (b)]. The example (d) summarizes well the situation. As long as the purity of the state decreases, it is advantageous to use a control field but when the purity starts increasing the dissipation alone becomes more efficient.

Finally, we point out that a visual inspection of the optimal syntheses allows to check the form of the reachable sets given in Sec. IV B.

## VI. CONCLUSION

We have investigated the time-optimal control of a two-level dissipative system. For different initial and final points, we have constructed the optimal syntheses which allow us to rigorously conclude on the beneficial role of the dissipation in order to reduce the duration of the process. An open question is the generalization of the present study to more complex quantum systems with for instance two control parameters or three levels. The determination of the optimal syntheses for these systems requires more sophisticated mathematical tools than those used in this paper [? ]. In addition, such an analysis could also be performed on other problems of quantum control. We point out that the question of measurement in the context of geometrical control theory is particularly interesting. Measurements can be viewed as a non-unitary control which allows to enlarge the reachable sets. For instance, we can consider systems not completely controllable by unitary control but which become controllable if measurements are used. A simple example is given by a finite number of levels of the harmonic oscillator with a constant dipolar interaction only between adjacent energy levels [? ]. From a formal point of view, this problem raises the challenge of the precise formulation of the Pontryagin maximum principle in this context which is to our knowledge an open question. We notice that all these geometrical tools would allow us to answer some physical relevant questions such as the time

at which measurements have to be done to minimize the duration of the control.

### APPENDIX A: THE CLOCK FORM

We derive in this section the expression of the clock form denoted  $\alpha$  [?]. By definition, the clock form is a 1-form which fulfills the following conditions

$$\begin{cases} \alpha(F) = 1 \\ \alpha(G) = 0 \end{cases} . \quad (\text{A1})$$

A solution of this system exists except on the set  $C_A$  where  $F$  and  $G$  are collinear. If we write  $\alpha$  as  $\alpha = \alpha_2 dx_2 + \alpha_3 dx_3$  then simple algebra shows that  $\alpha_2$  and  $\alpha_3$  are solutions of the system

$$\begin{cases} \alpha_2(-\Gamma x_2) + \alpha_3(\gamma_- - \gamma_+ x_3) = 1 \\ \alpha_2 x_3 = \alpha_3 x_2 \end{cases} . \quad (\text{A2})$$

We obtain that

$$\begin{cases} \alpha_2 = \frac{-x_2}{\Gamma x_2^2 - \gamma_- x_3 + \gamma_+ x_3^2} \\ \alpha_3 = \frac{-x_3}{\Gamma x_2^2 - \gamma_- x_3 + \gamma_+ x_3^2} \end{cases} . \quad (\text{A3})$$

From the 1-form  $\alpha$ , we can define the 2-form  $d\alpha$  which is given by

$$d\alpha = \left( \frac{\partial \alpha_3}{\partial x_2} - \frac{\partial \alpha_2}{\partial x_3} \right) dx_2 \wedge dx_3 , \quad (\text{A4})$$

and reads after some calculations

$$d\alpha = \frac{2\Gamma x_2 x_3 + \gamma_- x_2 - 2\gamma_+ x_2 x_3}{[\Gamma x_2^2 - \gamma_- x_3 + \gamma_+ x_3^2]^2} dx_2 \wedge dx_3 . \quad (\text{A5})$$

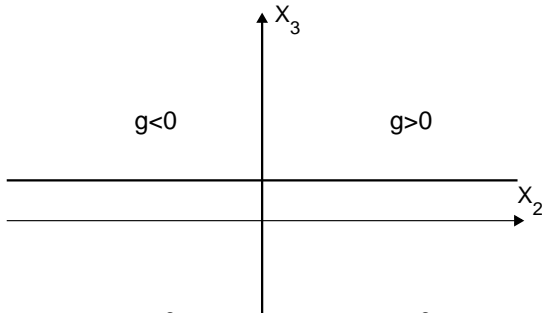
If we write  $d\alpha$  as  $d\alpha = g(x_2, x_3) dx_2 \wedge dx_3$  then one sees that  $g(x_2, x_3) = 0$  on  $C_B$  and that the function  $g$  has a constant sign in the regions delimited by the lines of  $C_B$ . This point is displayed in Fig. 9. As suggested by its name, the clock form is a form which allows one to determine the time taken to travel a path and to compare the extremals. Let  $\gamma$  be a path in the plane  $(x_2, x_3)$  which does not cross  $C_A$  and  $T$  the time of travel along  $\gamma$ . We have

$$\int_{\gamma} \alpha = \int_0^T \alpha(\dot{\mathbf{x}}) dt = \int_0^T \alpha(F) dt = T . \quad (\text{A6})$$

We consider now two paths  $\gamma_1$  and  $\gamma_2$  starting and ending at the same points and respectively associated to the durations  $T_1$  and  $T_2$ . One shows by using the Stokes theorem that

$$T_1 - T_2 = \int_{\gamma_1} \alpha - \int_{\gamma_2} \alpha = \int_D d\alpha , \quad (\text{A7})$$

where  $D$  is the surface delimited by  $\gamma_1 \cup -\gamma_2$ . For paths  $\gamma_1$  and  $\gamma_2$  which lie in one of the four quadrants defined by  $C_B$ , we can straightforwardly determine the time-optimal trajectory.



### APPENDIX B: ANALYTICAL DETERMINATION OF THE DYNAMICS

In this section, we solve analytically the dynamics of the system given by the following system of differential equations

$$\begin{cases} \dot{x}_2 = -\Gamma x_2 - u x_3 \\ \dot{x}_3 = \gamma_- - \gamma_+ x_3 + u x_2 \end{cases} . \quad (\text{B1})$$

We assume that  $u = \pm 1$  and we denote by  $u = \varepsilon$  the control term. Combining Eqs. (B1), one arrives to equations that depend on only one variable  $x_2$  or  $x_3$

$$\begin{cases} \ddot{x}_2 + (\Gamma + \gamma_+) \dot{x}_2 + (1 + \Gamma \gamma_+) x_2 + \varepsilon \gamma_- = 0 \\ \ddot{x}_3 + (\Gamma + \gamma_+) \dot{x}_3 + (1 + \Gamma \gamma_+) x_3 - \Gamma \gamma_- = 0 \end{cases} . \quad (\text{B2})$$

Equations (B2) are linear inhomogeneous differential equations of second order whose discriminant  $\Delta$  is given by

$$\Delta = (\Gamma - \gamma_+)^2 - 4 . \quad (\text{B3})$$

A qualitative change of the solutions is expected according to the sign of  $\Delta$ , i.e. a transition from a pseudo-periodic solution for  $\Delta < 0$  to an aperiodic solution for  $\Delta \geq 0$ . This point is summarized in Fig. 10. Note that the parameter  $\gamma_-$  plays no role in the structure of these trajectories but modifies their limits points. Simple algebra allows one to calculate the exact solutions. For instance for  $\Delta > 0$ , we obtain

$$\begin{cases} x_2(t) = e^{-(\Gamma + \gamma_+)t/2} [x_{20} \cosh(\frac{\delta}{2}t) - (x_{20} \frac{\Gamma}{\delta} - x_{20} \frac{\gamma_+}{\delta} + \frac{2\varepsilon}{\delta} x_{30}) \sinh(\frac{\delta}{2}t)] \\ x_3(t) = e^{-(\Gamma + \gamma_+)t/2} [x_{30} \cosh(\frac{\delta}{2}t) + (\frac{\Gamma - \gamma_+}{\delta} x_{30} + \frac{2\varepsilon}{\delta} x_{20} + \frac{2\gamma_-}{\delta}) \sinh(\frac{\delta}{2}t)] \end{cases}$$

where  $(x_{20}, x_{30})$  is the initial point of the dynamics and  $\delta = \sqrt{\Delta}$ .

### ACKNOWLEDGMENTS

The authors thank B. Bonnard and U. Boscaïn for many helpful discussions.

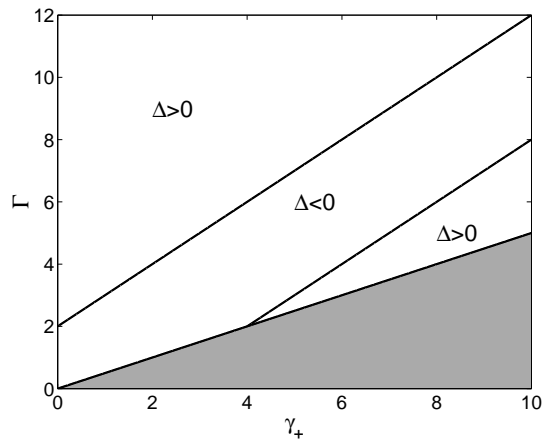


FIG. 10: Sign of the discriminant  $\Delta$  as a function of the parameters  $\Gamma$  and  $\gamma_+$ . The parameters are in arbitrary units. The zone in grey is excluded for Lindblad dynamics.